Results of the Antarctic VLBI experiments during JARE39 and their geodetic interpretations

Takaaki Jike

1. Introduction 6

2. Tectonics and current crustal movement in Antarctica 9
2.1 Introduction 9
2.2 Tectonics of Antarctica 9
2.2.1. Structure of the Antarctic crust 9
2.2.2. Geological characteristics of East Antarctica 10
2.2.3. Geological characteristics of West Antarctica 11
2.2.4. Summary of the geological characteristics 11
2.2.5. Seismicity in Antarctica 11
2.2.6. Interaction between the continental glacier and the crust 12
2.2.6.1 Global glacial model 12
2.2.6.2 The glacial model of Antarctica 12
2.2.6.3 Geological phenomena in the Syowa Station periphery 13
2.3 Current crustal movement in Antarctica 13
2.3.1. Tectonic setting 13
2.3.2. Current plate models 14
2.3.3. Prediction of intra-plate deformation 15
2.3.4. Detection of plate motion by space geodetic techniques 15
2.3.5. Detection of Post Glacial Rebound 16

3. The VLBI observation system and experiments at Syowa Station 20
3.1 Introduction 20
3.2 Roles of the Antarctic VLBI 20
3.2.1. Present environment surrounding VLBI 20
3.2.2. Significance of VLBI among space-geodetic techniques 21
3.2.3. Roles of VLBI observations for Antarctic geodesy 21
3.2.4. Present status of the Antarctic VLBI 22
3.3 Japanese Antarctic Research Expedition and past VLBI experiment at Syowa Station 23
3.3.1. Location of Syowa Station 23
3.3.2. Access to Syowa Station 23
3.3.3. Scientific activities in Syowa Station 23
3.3.4. Past VLBI observations at Syowa Station 24
3.4 Establishment of VLBI system for regular observations in Syowa Station 24
3.4.1. Outline of the VLBI project carried out by JARE39 24
3.4.2. Brief description of a VLBI observation system 25

3.4.3. VLBI observation system in Syowa Station 25
3.4.4. Fringe test before shipping 26
3.4.5. Construction of the VLBI observation system 26
3.4.6. Problems during the construction 29
3.5 Regular observations and their summary 30

4. Development of the software for the correlation and geodetic analysis 51
4.1 Introduction 51
4.2 Development of new software 51
4.2.1. Structure of the newly developed geodetic analysis system 51
4.2.2. Characteristics of processing by the MFC 52
4.2.2.1 Definition of delay used by the MFC 53
4.2.2.2 Characteristics of the output from the Mitaka FX Correlator 54
4.2.3. Bandwidth synthesis 56
4.2.4. Time system transformation 57
4.2.5. Summary of the newly developed software 60

5. Results of analysis and the geodetic interpretation 67
5.1 Introduction 67
5.2 Summary of correlation processing 67
5.3 Results of the analysis 68
5.3.1. Analysis setting 68
5.3.2. Coordinates of the Syowa VLBI reference point 69
5.3.3. Discussions on errors 70
5.4 Discussion for the clarification of error factors 74
5.5 Comparison with other estimations of Syowa's position and velocity 75
5.5.1. The first VLBI experiment at Syowa Station in 1990 by JARE30 75
5.5.2. ITRF2000 and the VLBI experiment in November, 1999 75
5.5.3. Velocity of IGS point in Syowa Station 76
5.5.4. Velocity predicted by a global plate motion model 77
5.5.5. Velocity of the Syowa DORIS station 77
5.5.6. Position and Velocity of the Syowa space geodetic observation points in ITRF2000 77
5.5.7. Intercomparison of the determinations 78
5.6 Geodetic interpretations 82

6. Summary and conclusion 93

Acknowledgements

This study was performed under the support of National Astronomical Observatory, National Institute of Polar Research, Japan Antarctic Research Expedition and the Antarctic VLBI project members.

I would like to express my cordial gratitude to Professor Seiji Manabe (NAO Mizusawa) for his helpful supports, beneficial guidance, continuous encouragement, valuable discuses regarding to the development of the geodetic analysis system, upgrading of VLBI parameter estimation software, offering of the opportunity to the participation to the Antarctic expedition team and domestic support during the JARE action period.

I am pleased to acknowledge Professor Kazuo Shibuya (JARE39 captain, NIPR) for his many supports regarding to equipment and operation of the Antarctic VLBI project, upgrading of the observation network, negotiations with the VLBI stations in foreign countries and the correlation office, advice regarding the application of the Syowa VLBI station. The author also would like to acknowledge valuable consideration and support of Professor Kiichi Moriwaki (JARE39 sub-captain, NIPR) during the preparing period and the summer operation period to construction of VLBI observation system.

The author is indebted to Dr. Yoshiaki Tamura (NAO) for creating the antenna operation program for Syowa Station, Dr. Katsuhisa Sato (NAO) for development of D-cal data acquisition and support to the domestic test of VLBI system, Dr. Katsunori Shibata (NAO) for operation of the FX correlator corresponding to the variable demands of the author.

I am favored to have assistance of Mr. Yoshihiro Fukuzaki (GSI, JARE40) who supported the preparatory VLBI observation in Japan and observations during the wintering and continuation of the Antarctic VLBI experiment in JARE40. I also would like to express his appreciation to Dr. Koichiro Doi (NIPR, JARE41) for his various and large domestic supports to the Antarctic VLBI experiment in Japan.

Prof. Koichi Yokoyama is acknowledged for his invaluable help in preparation of the manuscript.

The author wishes to thank Mr. Yukio Takahashi, Mr. Noriyuki Kurihara (CRL), Dr. Osamu Kameya, Mr. Seisuke Kuji, Mr. Kenzaburo Iwadate, Dr. Noriyuki Kawaguchi and Mr. Takeshi Miyaji (NAO) for their invaluable supports and helpful discussions.

I am grateful to Dr. David L. Jauncey for his helpful discussion and to Dr. John Reynolds, Prof. Peter McCulloch, Dr. Marco Costa, Dr. George Nicolson and Dr.

Jonathan F. H. Quick for their contributions to the Antarctic VLBI experiment.

I deeply thank all of the JARE39 members who enjoyed wintering life together, assisted me with their many experiences and gave many supports to the VLBI observation. Here, I record names of the members of JARE39 with gratitude.

Ken-ichiro Kusano, Takayuki Kishi, Takehiko Yasuda, Toshiaki Hukita, Kazuhisa Horikawa, Nozomu Ohkawara, Shoichi Okano, Kazuo Meki, Kazuyo Sakanoi, Tomomi Yamada, Keisuke Suzuki, Gen Hashida, Kazunori Kashiwabara, Hideyasu Kojima, Shigeru Aoki, Hiroshi Kaiden, Yoko Tono, Toru Yada, Kin-ichi Muramatsu, Hideo Handa, Tazutaka Yoshida, Sachio Masakawa, Kazuhiko Yamamoto, Yuji Kato, Takashi Kusaka, Hiroshi Kiriyama, Takayuki Kugure, Giichiro Ohno, Takahiro Miyata, Yukio Oda, Yasuhiro Sato, Shigemitu Iino, Tomoya Morita, Satoshi Ohshiro, Hiroyuki Ogawa and Tanaka Teruhito, Miwako Yoritaka, Akihiro Masuyama, Masao Iwata, Shuji Aoki, Toshinobu Machida, Yasuto Osanai, Tsuyoshi Toshima, Masaaki Ohwada, Toshiaki Tsunogae, Nobuyuki Arai, Naoki Washiyama, Akira Ishikawa, Masahiko Ootani, Kenji Kurosawa, Yasuhisa Yamamoto, Shigeru Hukuda, Shigemitu Kasai, Eishin Watanabe, Yoichi Sakurai, Kiyoaki Saito, Kazuhiko Minawa, Tomokazu Hokada, Maki Kuroki, Warwick A. Crowe

Finally, I would like to thank my family who always support me. I would not be able to accomplish this work without their continuous supports and encouragement.

Abstract

In order to reveal tectonics of Antarctica, the VLBI observation project was resumed by JARE39 after 8 year interruption since the first observation in 1990. In this expedition a standard VLBI system for operational geodetic observations was established at Syowa Station and regular observations were initiated. VLBI observation system was established during summer operation in January, 1998. Four VLBI experiments were carried out during the wintering. Various troubles that occurred in wintering caused to succeed only the experiment in November, 1998.

Two recording systems, K4 and S2, are used in Antarctic VLBI observations. The data are correlated with Mitaka FX correlator, since it is the only correlator that can process both K4 and S2.

New analysis software was developed for the Mitaka FX correlator capable of geodetic use. Main parts of development are the bandwidth synthesis and the time system transformation. By using these tools, the delays were obtained and analyzed to estimate the position of Syowa VLBI reference point.

The position of the Syowa VLBI point was estimated to be 1766194.143m, 1460410.932m and -5932273.353m with standard deviations of 2.9cm, 2.5cm and 6.2cm in x-, y- and z-components in the geocentric Cartesian system. These errors are larger than typical values of recent inter-continental VLBI experiments. Nevertheless, the estimated position, combined together with other VLBI determinations at different epochs, clearly shows the movement. The velocity of Syowa Station in the local topocentric frame is 0.53cm/y, 0.01cm/y and 1.17cm/y in the N-, E- and U-components and their errors are 0.22cm/y, 0.17cm/y and 1.00cm/y, respectively. This result is in good accordance with the global plate motion model and also shows uplifting which is not contradictory with the Post Glacial rebound.

It is necessary to confirm the reliability of this analysis system and the analysis result. Standard deviation of the post-fit residual is about 300 pico seconds, which is fairly larger than typical values. However, the reason of this large standard deviation is not yet revealed and left to the future research. A plan is proposed to distinguish possible error sources, namely, those specific to this experiment and those of the analysis system.

1. Introduction

Antarctica is a geologically distinct continent from the others and its characteristics have not been well revealed yet. The most remarkable characteristic is the existence of continental glaciers that cover 97% of the continent. To uncover the contributions of the continental glaciers to earth scientific phenomena is presently an important research subject. Among them, one of the most important in solid earth science is an interaction between continental glaciers and the crust. In fact, continental glaciers are acting upon the continent as huge loads pushing it down to as deep as about 1000 m. Many traces in dew rock areas show expansion of the continental glaciers in the past. Contemporarily, the crust is upheaving with the reduction of the continental glaciers.

In addition, study of figure and behavior of the under the continental glaciers is one of the aims of Antarctic solid earth science.

Usually, estimation of stress field by seismic focus analyses, measurement of crustal movement and geological surveying of traces of the past crustal activities are needed to elucidate Antarctic tectonics. Antarctica, however, is seismically very quiet. In fact, large earthquakes hardly occur in the continent, except in volcanic areas and plate boundaries. Furthermore, movement of the Antarctic plate is very small and, therefore, it has not been easy to measure it with a satisfactory accuracy. In addition, since dew rock areas would be very narrow even if all of them were combined, it is difficult to find geological traces of crustal activities. Above all, the severe environment has hindered human beings from extending earth scientific expeditions. Thus, we have not obtained enough information for revealing the tectonics of whole Antarctica.

In consideration of the above scientific conditions, a direct method to study the tectonics of Antarctica is to measure relative positions among dew rock areas distantly apart from one another with the accuracy of a few centimeters or better. Methods that meet this requirement are the space geodetic techniques. Observation networks of the space geodesy evolved rapidly in the last decade and, thereby, motion of the Antarctic plate has been detected. Currently, the research interest is being shifted from inter-plate motion to intra-plate deformation and even to more detailed deformation in the polar area.

Syowa Station is one of the largest earth scientific observation complexes in the world. It is located in a dew rock area and has several space geodetic observation facilities as well as other earth scientific instruments. In order to monitor long-term change of the position of Syowa Station, required is a reference point tied to the most stable terrestrial reference frame and a celestial reference frame realized by

extragalactic radio source positions. Among the existing space geodetic methods that are able to define their own geodetic reference points, Very Long Baseline Interferometer (hereafter referred to as VLBI) is unique one in the sense that it determines the position purely geometrically with respect to a celestial reference frame.

In late 1980's a multipurpose 11m antenna usable for VLBI was constructed in Syowa Station. The first VLBI observation was carried out in 1990. Thereafter, however, VLBI observation was discontinued for eight years because of the operational and access difficulties. In 1998, a program for monitoring earth scientific phenomena occurring in the Antarctic plate by establishing a geodetic reference point of Syowa Station was initiated by Japanese Antarctic Research Expedition 39th (hereafter referred to as JARE39). For this program, astandard VLBI observation system was installed and the Antarctic VLBI observation project was resumed. Furthermore, JARE39 includes operation of regular VLBI observations throughout a year and geodetic analysis of the data obtained through regular observations during wintering. Thus regular observations were started at this expedition and have been continuing thereafter. Australian, South African and Japanese stations have been participating in this project.

In the course of network establishment, we were faced with a problem of mutual incompatibility of the existing recording systems. Namely, S2 system was in use by the Australian and South African stations, while K4 system by the Antarctic and Japanese stations. Fortunately, the Mitaka FX correlator, hereafter referred to as the MFC, is able to handle both recording systems and, therefore, it was used to carry out correlation processing.

However, necessary geodetic analysis tools were not fully implemented in the MFC. Accordingly, we developed new geodetic analysis tools for reducing the data of the Antarctic VLBI project. It is to be mentioned that the MFC is non-standard in some respects. The most notable difference from other correlators used in geodesy is that it adopts geocentric time system in correlation processing. Therefore, we developed and installed a function of time system transformation.

The position of Syowa Station VLBI reference point was determined from the JARE39 data with the newly developed geodetic analysis system mentioned above and agreed well with the result of the observation in 1999 obtained with the use of a usual analysis system. Standard deviations are several centimeters.

In this thesis we first review geology of Antarctica and figure out geophysical significance of the Antarctic VLBI project. Then, we give descriptions of the VLBI observation facility newly installed at Syowa Station, regular and operational VLBI

observations in Antarctica, mixed correlation processing of geodetic VLBI observations using two different recording systems, namely, K4 and S2, in particular, putting emphasis on development of the new geodetic analysis system for the MFC. Finally, results of the Antarctic VLBI experiments in 1998 are described. Their geophysical interpretation is made in combination with the VLBI results obtained at Syowa Station in 1990 and 1999 and the movement of Syowa VLBI reference point is compared with the velocities of crustal movement that are determined at the space-geodetic observation points of Syowa Station.

2. Tectonics and current crustal movement in Antarctica

2.1 Introduction

In order to understand tectonics of any region, stress fields and crustal motions, at present and in the past, have to be revealed. Usually, geological survey, seismic observations, and geodetic survey are used for this purpose. In particular, detection of crustal movement by geodetic observation is one of the most effective means. This is the case for Antarctic research.

Unfortunately, the sites which allow us to measure the crustal motion directly are limited to dew rock areas. Since dew rock areas are located along the coast of the Antarctic continent, lengths of baselines spanning two dew rock areas are typically of continental size. Accordingly, we need geodetic techniques to directly measure baselines of continental size with high accuracy along with geodetic measurement strategy.

The space geodetic techniques meet this requirement and observation points have been deployed in recent years. In the following, geological characteristics and results of the space-geodetic observations in Antarctica are described.

2.2 Tectonics of Antarctica

2.2.1. Structure of the Antarctic crust

The crustal structure of Antarctica almost corresponds to large-scale geological structure. The geological classification of Antarctica by Craddock (1972, 1982: see Science in Antarctica 9, 1985) is most widely used. Here, we briefly describe the geological characteristics of East and West Antarctica on the basis of Craddock's classification

Antarctica can be divided into East Antarctica and West Antarctica according to the structural characteristics. East Antarctica is the area enclosed by the coast from the west boundary of Ross Sea to the east boundary of Weddell Sea and the Transantarctic Mountains. West Antarctica is the area which includes Ross Sea, Ellsworth Land, Marie Byrd Land, and Antarctic Peninsula. Figure 2.1 shows the arrangement of east and west Antarctica.

Most part of East Antarctica consists of a continental shield. In fact, East Antarctica was part of a super continent. Although most of the continental crust is pushed down by the continental glaciers, the surfaces of base rocks are higher than the sea surface in many places (Atlas Antarktiki of the Soviet Union, 1977, see Science in Antarctica 9,

1985).

On the other hand, West Antarctica shows a distinct contrast to East Antarctica. Even if the continental glacier were removed and thereby the area were uplifted, the base rocks would be still lower than the sea surface in most of this area except for Antarctic Peninsula and several mountain regions. Ross Sea and Weddel Sea are mutually connected and many islands are hidden under the continental glaciers. These facts show that an evolutional process of West Antarctica is largely different from that of East Antarctica.

Antarctica is surrounded by Antarctic Ocean and is distantly apart from other continents. As is well accepted, the ocean was formed by expansion of the oceanic bottom. The forming process of the ocean is related to the evolution of the Antarctic plate accompanying with the disunion of Gondwanaland.

2.2.2. Geological characteristics of East Antarctica

Generally, a rock is refreshed by fluctuation. Accordingly, discovery of old rocks implies that there was no fluctuation after forming of the old rocks or motion that carried the rocks near the ground.

The continental shield of East Antarctica preserves very old rocks, which consist of granite and metamorphic rocks created in the Precambrian era. Especially, there are places where old rocks of isotope ages older than 2500Ma (1Ma= 1 million years ago) are found. This age corresponds to Archean. Furthermore, the area classified to Napier Complex, together with Greenland is particularly interesting, as it preserves rocks originated from the oldest crust. The oldest rock discovered in this area is speculated to be formed about 3500Ma.

There must have been large fluctuations when a continent disunited. East Antarctic shield is considered to be the central part of Gondwanaland (Craddock, 1982: see Science in Antarctica 9, 1985). In the course of the disunion of the huge continent, Africa and India began first separation around 180 Ma, then Australia disunited around 38Ma, and thus East Antarctica became the form similar to the present one. However, the latest fluctuations in East Antarctica confirmed by geological surveys are the Ross orogeny (450-520Ma, Kojima and Saito, 1978, see Science in Antarctica 9, 1985) and the Queen Maud fluctuation (400-620Ma, Kojima and Saito, 1978, see Science in Antarctica 9, 1985). Accordingly, it is considered that no large fluctuation has occurred in East Antarctica since Gondwanaland disunited.

In addition, the cause of the upheaval of the Transantarctic Mountains is one of the interesting subjects in the Antarctic science. The mountains are in the boundary area of East and West Antarctica. Webb et al. (1987) suggests that this area was uplifted

sharply after Tertiary (see Science in Antarctica 1, 1991).

2.2.3. Geological characteristics of West Antarctica

West Antarctica is more active than East Antarctica from the viewpoints of earth sciences. The geological structure of this area is characterized by superposition of several geological units generated by fluctuations newer than the Paleozoic era.

The area from Antarctic Peninsula to Marie Byrd Land is one of the geological units composing West Antarctica and runs along the edge of the East Antarctic shield. The new volcanic rocks and sediment rocks are distributed on the base layers. It is considered that these rocks are formed in Tertiary or Quaternary and the base layers were formed before the period when Gondwanaland disunited.

This area is the youngest geological unit of Antarctica and belongs to the Andean orogenic zone which was active from the late Mesozoic era to the Cenozoic era. This unit shows the structure connected to Andes through South Sandwich Islands and South Georgia Islands. Especially, the structure of Antarctic Peninsula remarkably resembles that of a plate subduction zone. For example, South Shetland Islands is located at the top of the Antarctic Peninsula and shows an active volcanic arc.

With respect to Ellsworth Land crossing the boundary of East Antarctica, the feature common to the geological unit of Cape Town periphery has been confirmed. It is conceivable that Ellsworth Land consists of a micro plate, which used to be connected to Antarctica when the Antarctic plate was formed.

2.2.4. Summary of the geological characteristics

There exist remarkable differences between East and West Antarctica, in their geological activities and structures. Namely, East Antarctica is geologically quiet after the disunion of Gondwanaland and its tectonic structure is rather simple. On the contrary, West Antarctica formed by several geological units is still continuing crustal activities. The above differences lead us to interesting research subjects, such as relative motions of geological units and interaction in the boundary areas.

2.2.5. Seismicity in Antarctica

Locations of seismic foci in Antarctic region are shown in figure 2.2. Based on this data, Kaminuma (2000) summarized the characteristics of the seismic activities in Antarctica. He classified the characteristic seismic activities into three types, namely, seismicity in plate boundary areas, intra-plate seismicity, and microseismic activities.

Almost all of the earthquakes in Antarctic region occur in the plate boundary named Circum Antarctic Seismic Belt. These earthquakes are due to expansion of the Antarctic plate or, in other words, transform faulting. On the other hand,

subduction-type earthquakes exceptionally occur at the top of Antarctic Peninsula.

In the intra-plate area, seismic activity is extremely low. As an exceptional case, a great earthquake with Ms 8.0 struck the Balleny Islands region on March 25, 1998 (figure 2.2). This intra-plate earthquake is the largest one ever recorded in the Antarctic plate. There were other earthquakes with magnitudes larger than 5.5 (Wiens et al., 1998; Tono and Kamimura, 1998) and a few large earthquakes before this event. In general, seismically active areas are limited to two active volcanic regions, namely, subduction type volcanoes located in the South Shetland Islands area and hot spot type volcanoes located in McMurdo Inlet.

Microseismic activities around Syowa Station were reported by Kaminuma et al. (1998). The epicenters of these microearthquakes are located in the coastal and offshore regions. As for crustal movements around Ongul Islands, block motional uplift of the crust and recovery of isostasy by deglaciation are associated with these earthquakes, as well as changes of oceanic level and elevation of the coast uncovered by leveling survey.

2.2.6. Interaction between the continental glacier and the crust

2.2.6.1 Global glacial model

Isostatic recovering after the latest deglaciation causes crustal deformation called Post Glacial Rebound (PGR). This phenomenon has been studied in Scandinavia and Five Large Lakes periphery since 1950's. In these areas, the crust has been rising for 10000 years after the extinction of the continental glacier. Currently, the vertical velocity is from 1 to 10 mm/y in the central region of Scandinavia. PGR is closely related to viscoelastic properties of the upper mantle. The deglaciation also gives rise to eustatic sea level change. Accordingly, measurement of PGR deformation rate is very important in view of determining the mantle structure and the scale of the continental glacier in the last Ice Age.

Tushigham and Peltier (1991) proposed a global model of the late Pleistocene deglaciation (ICE-3G) based upon post-glacial relative sea level changes. Then, Peltier (1994) improved this model in the northern hemisphere. This model, called ICE-4G, is useful for estimating crustal deformation in the North Polar region.

2.2.6.2 The glacial model of Antarctica

The global glacial model in the Antarctic region has not been renewed after ICE-3G. Presently, large continental ice-sheet covers base rocks in Antarctica. Although the whole history of its evolution is not clear, it is considered that the continental glacier once covered the whole continent including the dew rock areas in the latest glacial age.

On the other hand, Yoshida (1983) claims that this model over-estimated the glacial scale. In general, the continental glacier pushes down the crust by about 1000m as a load. In particular, expansion of continental glacier in the ice age caused increment of extra load to the crust. The traces formed by glacial erosion suggest certain advance of the continental glacier in the latest glacial age. However, improvement of the advance model of the continental glacier in Antarctica is a future subject.

2.2.6.3 Geological phenomena in the Syowa Station periphery

In the Syowa Station periphery, traces of seashore lines are left in bedrocks. Ancient marine deposits are confirmed above the sea level. They provide us with useful data for estimating relative sea level change and crustal rise. In Ongul Islands, the age of the shellfish fossil discovered in the marine deposit 20m above the sea level (Yoshida, 1985: Science in Antarctica Vol. 5) was estimated to be 6000y by the radiocarbon method. Such fossils have also been found in dew rock areas. Kaminuma et al. (1985: Science in Antarctica Vol. 5) estimated the uplifting speed of Syowa Station periphery to be 0.4cm/y.

Accordingly, development of the Antarctic crust is closely related to evolution of the continental glacier. Thus measurement of the contemporary crustal movement provides us with important information for understanding interaction between the continental glacier and the crust. It is especially interesting to make comparative study with the case of the northern hemisphere where the continental glaciers have almost faded.

2.3 Current crustal movement in Antarctica

2.3.1. Tectonic setting

Inside of the Circum Antarctic Seismic Belt is called Antarctic plate. A basic model of the Antarctic plate has been derived from research of seismicity and paleomagnetic anomaly in Antarctic Ocean. Most of the boundaries that enclose the Antarctic plate are ridges and transform faults, and the movement of the Antarctic plate is estimated to be extremely small. Since the Antarctic plate dose not subduct under other plates, it is considered that this plate is expanding. In addition, it is assumed that the expansion rate of the Antarctic plate area is about 5×10^4 km^2/10^6y.

According to Kubo et al. (1998), a tectonic setting of the Antarctic plate is explained to be adjacent to other six plates. They are Australian, Pacific, Nazca, Scotia, South American, and African plates. The plate surrounding the Antarctic plate is shown in figure 2.3. The spreading rate adopted in the NUVEL-1 (DeMets et al., 1990)

kinematical plate model ranges from 1 to 10 cm/y. Relative motion of the Antarctic plate with respect to Australian, Pacific and Nazca plates is faster than 4cm/y, and slower than 4cm/y with respect to Scotia, South American and African plates, respectively.

Currently, existence of several micro plates along the plate boundaries is assumed for explaining kinematics of the Antarctic plate. For example, Phoenix microplate collides against the Antarctic plate at the offshore of South Shetland Islands and forms only one subducting zone (South Shetland Trench) in Antarctica. In this field, a number of surveys have been conducted with respect to seismicity and oceanic magnetic anomalies. Larter and Barker (1991) estimated the velocity of Phoenix miroplate to be roughly 2cm/y by an analysis of oceanic magnetic anomalies.

On the other hand, DeMets et al. (1988) proposed a hypothetical microplate moving toward the triple junction of Pacific, Australian, and Antarctic plates on the basis of the focal mechanism of earthquakes that occurred along the transform fault extending from New Zealand. The stress field of this area is conjectured from the relative motion of the Antarctic plate and the hypothetical microplate. However, the focal mechanism of the Balleny Islands event on 25 March 1998 was inconsistent with hypothetical stress field.

2.3.2. Current plate models

Existing plate motion models which are based on paleomagnetic data spanning millions of years have been found to implement a good quantitative characterization of the present-day plate motion.

The first global plate motion model was presented by Minster and Jordan (1978), denoted AM0-2, and was readily incorporated in VLBI analysis software. More recent models, denoted NUVEL-1 and NNR-NUVEL-1, are due to DeMets et al. (1990) and Argus and Gordon (1991), respectively. NUVEL-1 was determined from transform fault azimuths, earthquake slip vectors, and spreading rates estimated from oceanic magnetic anomalies which are clues of motions over the past three million years. Plate motions are expressed relative to the movement of Pacific Plate. NNR means no-net-rotation and the NNR condition is such that $\mathbf{v} \times \mathbf{r}$ integrated over the surface of the Earth is constrained to be zero. Here, $\boldsymbol{v}$ is a velocity at a point $\boldsymbol{r}$ on a rigidly rotating tectonic plate. Successively published models are NNR-NUVEL1-A (DeMets et al., 1994) as an updated version of NNR-NUVEL1, and HS-NUVEL-1 (Gripp and Gordon, 1990) based on the model of plate velocities relative to hotspots. The model we mainly used in this thesis is NNR-NUVEL1A.

If we assume that the Antarctic plate consists of a sheet, the velocity of Syowa

Station is easily predictable by a global plate motion model. The angular velocity of the Antarctic plate given by NNR-NUVEL-1A is less than a tenth of that of Cocos plate which is speculated to be moving fastest. In addition to this, since the Euler pole of the modeled Antarctic plate is directed toward Syowa Station, crustal movement by plate motion of the Syowa Station periphery is predicted to be very small.

The NNR-NUVEL1A model is compared with the Antarctic plate motion estimated from the space geodetic observations, namely, VLBI and GPS. Results of comparison will be described later.

2.3.3. Prediction of intra-plate deformation

The difference of the movement in East and West Antarctica was suggested by Molnar et al. (1975). They suggested that East Antarctica is moving differently from West Antarctica. If this is the case, we need to know whether the relative motion is caused by intra-plate deformation or by motions of several plates corresponding to geological units.

Difference is also seen in the seismic structure of the lithosphere beneath the continent. If geological activities which divided Antarctica clearly to the eastern and the western part are still continuing, present plate motion models and evolution models of Antarctica have to be modified.

Kubo et al. (1998) suggested relevancy of focal mechanism of the Balleny Islands event and possibility of decoupling deformation between East and West Antarctica based on the assumption that the boundary of East and West Antarctica grows to the Balleny Islands area. Also, Kubo et al. (1999) explained it by shear wave splitting anisotropy beneath the Antarctic upper mantle and showed its possible formation process.

2.3.4. Detection of plate motion by space geodetic techniques

In recent years, several space-geodetic observation points have been deployed in Antarctica. Heki (1999) summarized motion of the Antarctic plate obtained by two space-geodetic techniques, namely, GPS and DORIS (Doppler Orbitography and Radiolocation Integrated by Satellite).

GPS observation points of IGS (International GPS Service) have been established at several stations in Antarctica since the beginning of 1990's. Syowa Station has been continuously observing since JARE36 (1995). Larson et al. (1997) first estimated the three components of the Euler pole of the Antarctic plate by using GPS data of three IGS points. Subsequently, Yamada et al. (1998) estimated the parameters of the Euler pole together with velocities of six IGS stations on the Antarctic plate and one station on the boundary between the Pacific plate and the Australian plate. They concluded

that the Antarctic plate is moving almost as a rigid plate, and Syowa Station is located on the stable interior of the Antarctic plate.

Observation stations of the DORIS system operated by CNES with the participation of IDS (International DORIS Service) of France are deployed in Terre Abele, Marion Is., Kerguelen, Rothera and Syowa Station on the Antarctic plate. Cretaux (1998) estimated the parameters of the Euler pole from the horizontal velocity vectors of the five DORIS stations. Discrepancies of velocities between predictions by NNR-NUVEL-1A and observations at space-geodetic stations in Antarctica are not systematic and smaller than 1cm/yr at the present. Since space geodetic observations in Antarctica cover only a decade of observation period, it is necessary to continue to monitor changes of velocity vectors by accumulation of observations. In addition, in order to identify systematic difference between models and observations and thereby to understand tectonics of Antarctica, exclusion of error sources stemming from observation systems is still to be pursued.

Kubo et al. (1998) suggested possible relative motion between East and West Antarctica. This was inferred from anomaly of residual velocity in McMurdo by subtracting fitted rigid plate motions of the Antarctic plate. However, as McMurdo is located near a volcanic area, there remains a possibility that volcanic local movements affect the motion in this area.

2.3.5. Detection of Post Glacial Rebound

Soudarin et al. (1999) compared the DORIS data with the PGR model based on ICE-4G but found no significant consistency between them. Normally with regard to space geodetic techniques, the error in the vertical component is larger compared with those of horizontal components Thus we are facing a difficulty for more reliable determination of the vertical motion by means of space geodetic techniques, and hence future improvement is absolutely necessary.

There has been so far no reliable evidence of the PGR in Antarctica. The predicted vertical velocity of PGR is about 0.5 – 1cm/yr and this amount is considered to be observable as the changing rate of distant baseline lengths in the global network. Hence long term and regular observations, by means of VLBI, is extremely important. Odamaki et al. (1991) discussed annual means of MSL (mean sea level) at Syowa Station from 1981 to 1987 based on tide gauge data. The sea level change was estimated to be 0.95cm/y. This result is larger than the one obtained from the geological survey (Kaminuma et al. 1985). Odamaki et al. (1991) also mentioned that longer observations are necessary for obtaining a definitive conclusion.

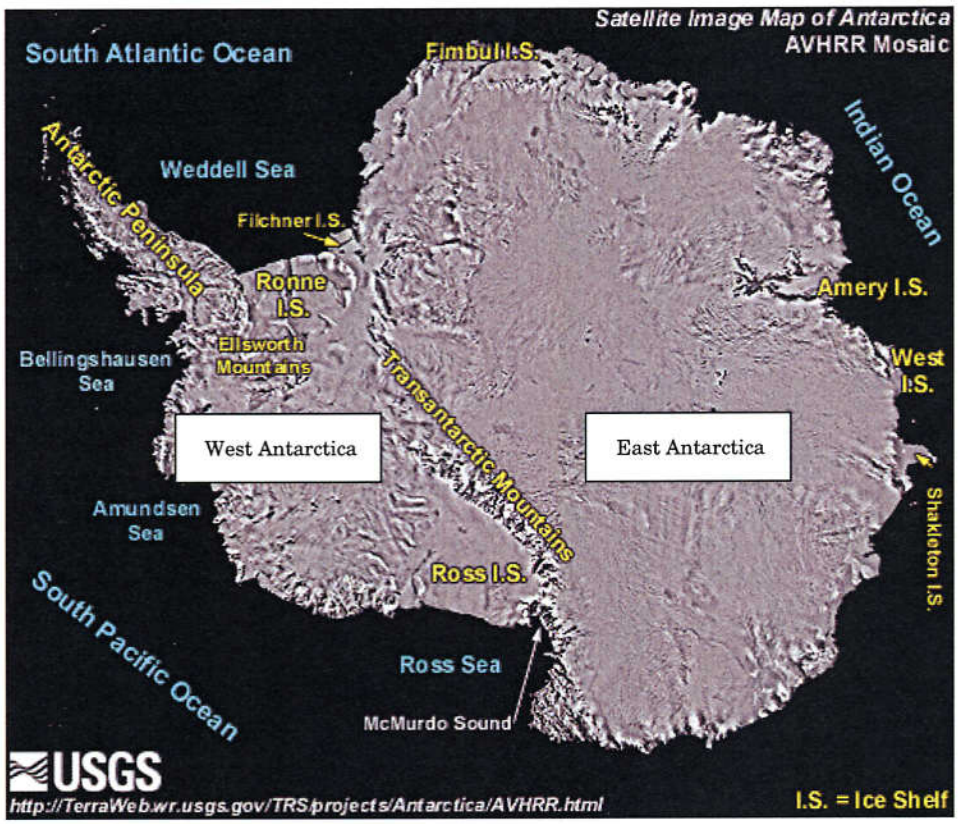

Figure 2.1. The arrangement of geographical structures in Antarctica. East Antarctica is the eastern hemispher side and West Antarctica is the western site of Antarctica. The Transantarctic Mountains is the boundary between East and West Antarctica.

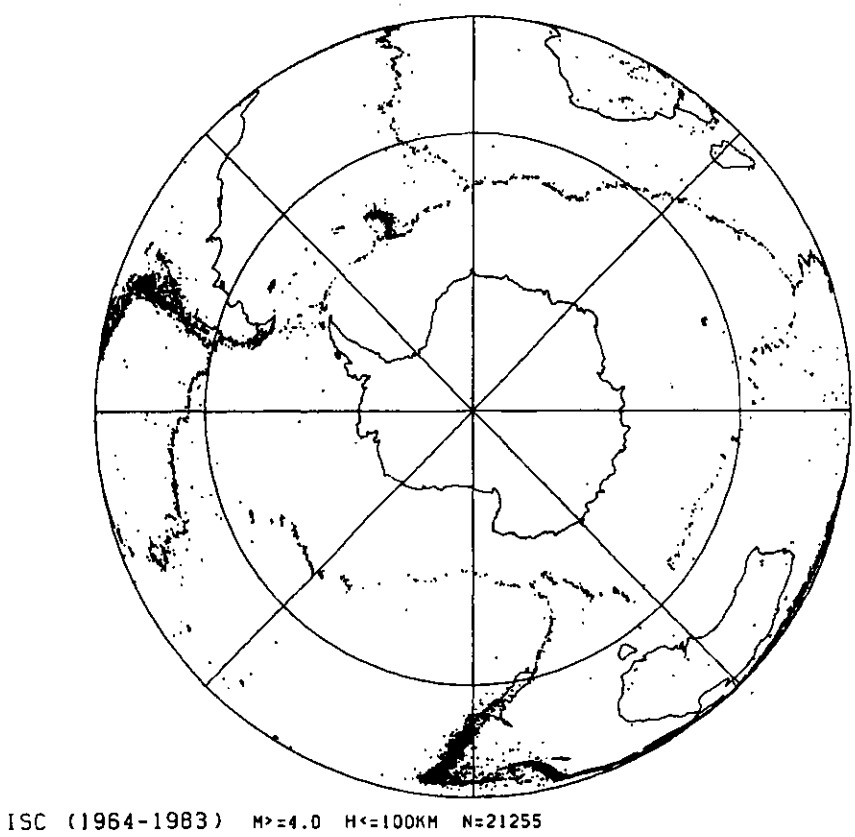

Figure 2.2 Distribution of seismic foci in the Antarctic region

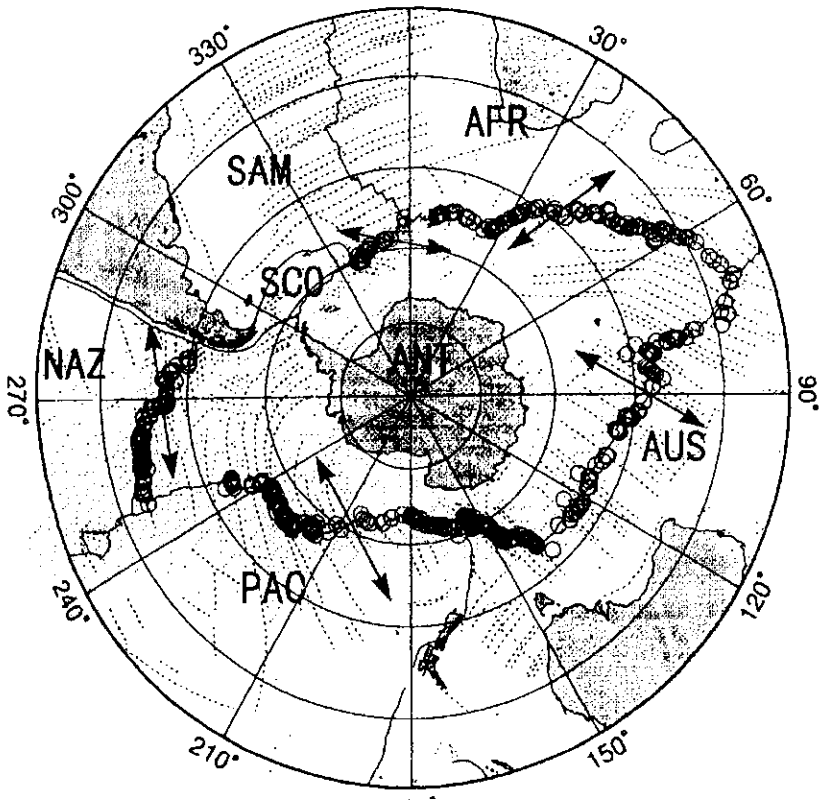

Figure 2.3 Plate configuration and epicenters of the circum Antarctic area by Kubo et al. (1998). Solid and dashed lines indicate plate boundaries and fracture zone, respectively. Arrows are typical directions of relative plate motions. Open circles are epicenters.

3. The VLBI observation system and experiments at Syowa Station

3.1 Introduction

VLBI experiments during wintering period began at Syowa Station for the first time in the world, as an important observational activity supporting Antarctic sciences. The project was initiated in JARE39 (Japanese Antarctic Research Expedition 39th). Missions of JARE39 are to establish VLBI observation system at Syowa Station, to start regular geodetic VLBI observations and to analyze VLBI data obtained during one year. The author joined JARE39 as a wintering member and started the regular Antarctic VLBI experiment at Syowa Station.

In the following, current status of geodetic VLBI in general and roles of Antarctic VLBI are reviewed. Then, described will be the VLBI system at Syowa Station constructed during JARE39, characteristic of the Antarctic VLBI observation network configuration, and results of regular observations.

3.2 Roles of the Antarctic VLBI

3.2.1. Present environment surrounding VLBI

The first geodetic VLBI observation was made in 1980, and then observation networks have evolved rapidly in the 1980's and are continuing to evolve. During these two decades, VLBI technique has accomplished fundamental contributions in geodesy and geophysics. This is due to achievement of dramatic accuracy improvement of more than two orders of magnitude in positioning on the surface of the Earth. For example, variations of polar motion, UT1 and L.O.D (length of day), and precession/nutation, helped increase our knowledge rapidly with respect to interactions among the atmosphere, the ocean and the solid Earth including deep interior like the outer and the inner core. This brought about a new discipline like earth system science. Another example is the detection of contemporaly plate motions and stepwise displacements associated with crustal movements due to Earthquakes.

VLBI was the most accurate space geodetic technique until the first half of 1990's when GPS (Global Positioning System) proved its promising capability in the precision geodesy. Further, new space geodetic techniques using artificial satellites has grown rapidly since the second half of 1990's. These techniques are capable of obtaining geodetic data by taking the advantage which VLBI does not have. For example, GPS is able to produce geodetic data with higher temporal and spatial resolution and with

lower cost for observation and data handling. DORIS ground station is composed of simple equipment that transmits the beacon to the artificial satellites, and more than 50 ground points are developed with the earth scale. InSAR (Interferomeric Synthetic Aperture Radar) is also able to detect two-dimensional regional deformation of the Earth's crust with comparable accuracy, although its result of observation is limited to the relative fluctuation in a narrow area.

However, growth of the geodetic techniques by means of artificial satellites does not mean that VLBI can be substituted by satellite techniques. VLBI has its own application to geodesy and geophysics, compared to other space geodetic techniques.

3.2.2. Significance of VLBI among space-geodetic techniques

Global geodetic techniques including VLBI refer to positions in ITRF (International Terrestrial Reference Frame) and ICRF (International Celestial Reference Frame). Among the space geodetic techniques, VLBI is unique in the respect that it observes natural celestial bodies which look almost at rest as references and determines positions of reference points on the Earth directly and geometrically.

On the other hand, other space-geodetic techniques use the orbit of artificial satellites as the references. This means that the fluctuation of the gravity center of the earth affects to the orbital motion. Namely, the reference systems of space geodetic techniques using artificial satellites depend on fluctuation of the gravity field.

The positions of celestial bodies refer to the ICRF which is considered to be the best realization of the inertial frame and is therefore more stable than other frames that use orbits of artificial satellites as references. Thereby the position obtained by VLBI is most suitable as a reference to other space geodetic reference points and geophysical observation instruments.

3.2.3. Roles of VLBI observations for Antarctic geodesy

In order to clarify tectonics of some region, crustal movement obtained from the geodetic survey, focus analysis of earthquakes and analysis of stress field are used. However, as described in Chapter 2, the seismic activity of Antarctic regions covered by the continental ice sheet is extremely low. This, results in difficulty of getting geophysical data from seismic observations. In the Antarctic area, information of the crustal movement is relatively more important than that in other regions. Thus VLBI is expected to play a significant role, since it can determine the crustal movement accurately.

Significance of VLBI observations at Syowa Station can be summarized as follows.

1) The role as a reference station to geodetic observation points in Antarctica

Syowa Station is operating several different space geodetic instruments, namely, VLBI, GPS, DORIS and PRARE (Precise Range And Range-Rate Equipment). In addition, tide gauge and leveling survey are also running. Since these instruments are located on a common base rock, intercomparison of the data should enable us to extract essential phenomena related to Antarctic sciences with high reliability. The most important role of VLBI is to determine the ITRF frame with high accuracy for use by other space geodetic techniques and also by other geophysical measurements.

2) Contribution to construction of a celestial reference frame

The number of existing VLBI stations in the southern hemisphere is not sufficient yet and the latitude of Syowa VLBI station is the highest among them. Accordingly, a considerable contribution is expected regarding construction of a celestial reference frame in the southern hemisphere.

3) Contribution to tectonics of Antarctica

The area where Syowa Station is located belongs to a geologically stable continental shield. In addition, as this area is far from the plate boundary, it is supposed that the crustal movement is stable and can be well approximated by plate motion models. On the other hand, the Antarctic plate motion model is evolving from the single rigid-plate model to multi-plate one. Recently, in fact, detection of intra-plate deformation and/or decoupling of East and West Antarctica are recognized as interesting subjects for understanding evolution of the Antarctic plate. Fortunately, since two VLBI stations in Antarctica, namely Syowa and O'Higgins, are located in East and West Antarctica, respectively, determination of relative movement between them will give a reasonable restraint to the motion and the deformation of Antarctic Plate.

3.2.4. Present status of the Antarctic VLBI

The Antarctic VLBI requires special considerations that are not necessary for VLBI in other continents. First, Antarctica is the continent 97 % or more of which is covered with the ice sheet. This ice sheet makes it difficult to discriminate plate tectonic crustal movement from local or regional deformation. Second, the accesses from other continents are almost impossible in the winter season. This limits the materials and personnel available in wintering. The wintering party must conduct many operations in their station under such restrictions.

Only a few large-scale stations are possible to operate the VLBI equipments such as a large parabolic antenna. At present, only two stations, Syowa and O'Higgins in

Antarctic Peninsula, are equipped with VLBI facilities but the increase of the VLBI stations cannot be expected in the near future.

3.3 Japanese Antarctic Research Expedition and past VLBI experiment at Syowa Station

3.3.1. Location of Syowa Station

The Japanese Antarctic station "Syowa" (69.0° S, 39.5° E) is located in East-Ongul Island, Soya Coast area, Lützow-Holm Bay, East Antarctica (Figure 3.1). East-Ongul Island belongs to Ongul Islands and is the second largest island next to West-Ongul Island. Ongul Islands is one of the dew rock areas around Lützow-Holm Bay. Syowa Station is built on bedrock.

3.3.2. Access to Syowa Station

Syowa Station is accessible only once a year by an icebreaker ship called Shirase (Figure 3.2). It takes nearly five months to go to and from even for the summer operation, while the wintering requires seventeen months. Nevertheless, more than forty members stay as a wintering party and about twenty members join as a summer operation party every year. Shirase stays near Syowa Station during the summer operation, namely, from the end of December to the beginning of next February.

3.3.3. Scientific activities in Syowa Station

Syowa Station was established in 1967 and has been maintained by NIPR (National Institute of Polar Research) almost for forty years. Now, Syowa Station has grown up to one of the largest stations in Antarctica and continuously performs Earth scientific observations.

NIPR organizes JARE (Japanese Antarctica Research Expedition) and dispatches JARE members to Antarctica every year. Scientific activities of JARE cover wide fields including meteorology, geomagnetism, geology, biology, seismology, geodesy, oceanography, meteorite survey, geochemistry, glaciology, geomorphology, cartography, auroral physics and ionosphere sciences. Activities during one year are divided into the summer operation and the wintering. The summer operation consists of preparation for regular observations to be carried out during the wintering and project observations specified for the summer operation. Missions during the wintering are regular observations in Syowa Station, field works and project observations of the wintering plan.

3.3.4. Past VLBI observations at Syowa Station

JARE30 (1988-1990) constructed the 11m parabolic antenna in Syowa Station. This antenna is called "Multipurpose 11m Parabolic Antenna" (MPA). The antenna was designed so as to be usable for VLBI, although its primary purpose is to receive signals from artificial satellites passing over the Antarctic region. This antenna had been the only VLBI antenna VLBI until O'Higgins station equipped the second one.

The front-end system was developed in 1989 and several radio sources were observed. S and X bands are simultaneously observable for use in standard geodetic VLBI experiments. VLBI back end system (K-4 system) was brought into Syowa Station in the period of JARE31 (1989-1991) summer operation. A crystal-cesium clock was used as a frequency standard instead of a hydrogen maser frequency standard.

Two experimental VLBI observations ware carried out on January 20 and 25, 1990 among Syowa Station, Tidbinbilla in Australia and Kashima 26m in Japan. The back-end system and observation tapes were brought back to Japan in April 1990. The correlation and data reduction were done at CRL Kashima.

Kurihara et al. (1995) estimated the position of the Syowa VLBI reference point with an error of several cm and summarized causes of this large error as follows.

1) Commonly visible area among the antennas in azimuthal direction was limited, since the network consisted of only very long baselines (longer than 6000km).

2) The elevation coverage of sky could not be wide enough. Accordingly, the error of the vertical component became larger compared with the horizontal one.

3) Stability of the frequency standard was not satisfactory because of large change of ambient temperature of the frequency standard.

After these observations finished, logistic difficulties and severe observational environment made subsequent VLBI observations abandoned until 1998. Furthermore, VLBI observation units, which are parts of front-end system, all units of back-end system and the frequency standard, were brought back to Japan.

3.4 Establishment of VLBI system for regular observations in Syowa Station

3.4.1. Outline of the VLBI project carried out by JARE39

JARE39 started a three-year project of VLBI experiments at Syowa Station from February 1998 by using the MPA. This project is called "Syowa Experiment" and it is the first observation using standard VLBI observation system in Syowa Station. The

period of JARE39 is the first year of this project.

The roles of JARE39 are: 1) establishing the VLBI observation system and its operation in wintering, 2) enforcing the observation in wintering, 3) collecting problems which may occur during the operation, 4) enabling geodetic use of the Mitaka FX Correlator. Preparation for the long time operation of the Syowa experiment is also an important subject.

In this project, regular experiments are aimed among Syowa Station, Hobart (University of Tasmania, Australia) 26m antenna, and Hartbeesthoek Radio Astronomical Observatory (South Africa, abbreviated as HartRAO) 26m antenna. These antennas form a core network of this project and some antennas (Kashima 26m antenna in Japan and Parkes 64m antenna in Australia Telescope National Facility) occasionally participated in the experiment (Figure 3.3). Four experiments per year and 48 hours session for each experiment were scheduled in this project.

The Syowa experiment network has a special characteristic in compatibility of recording systems. There are several kinds of VLBI recording systems in the world. For example, Mark-Ⅲ, Mark-Ⅲa, Mark-Ⅳ, VLBA, K4 (and its variants) and S2 systems are practically used for geodetic and astrophysical purposes. There is no compatibility among the recording systems usually. Therefore, when we plan worldwide network VLBI experiments, the difference of the recording system gives rise to serious problems. In Syowa Experiment in 1998, Syowa and Kashima used K4 system, while Hobart, HartRAO and Parkes used S2 system (Figure 3.4).

The incompatibility of different systems is resolved in the correlation process. The Mitaka FX Correlator at NAO (National Astronomical Observatory, Japan) can process cross-correlation between K4 and S2 tapes. S2 tapes are copied to K4 tapes with TSS (Timing Synchronize Signal) beforehand with correlation. Syowa experiment is the first occasion to combine the K4 and S2 systems in geodetic VLBI experiments.

3.4.2. Brief description of a VLBI observation system

The VLBI observing equipment usually consists of three parts as shown in figure 3.5. The first one (front-end system) is a large parabolic antenna fixed to the Earth's crust and used to receive weak radio wave radiated by celestial bodies. The second one (back-end system) is a terminal that records the signals received by the antenna. The signals are digitized by a high-speed A/D converter and recorded by a high-speed recorder. The third one is a frequency standard which supplies very stable reference signals to other instruments used in observation.

3.4.3. VLBI observation system in Syowa Station

MPA (figure 3.6) at Syowa Station is designed as a multipurpose satellite data

receiving system and a geodetic VLBI system. The S and X band receivers have standard specifications for geodetic VLBI observations. The slew speed is high because the antenna is designed to track artificial satellites.

The VLBI back-end system in Syowa Station is called K4-TCU (Timing Control Unit) system. This system is often called by other nicknames of K4-TSS or 4-VSOP. K4-TCU is necessary for time synchronous processing by the MFC. It has two time signals; one is time tag written in observed data directory and another is TSS-ID. This enables correlation by using K4 correlator in GSI (Geographical Survey Institute, Japan).

Three PC's are used in this system. The first one is used for VLBI field system, which controls the recorder. The second one is used for pointing control of the antenna and last one is used for calibration of cable delay.

Two hydrogen masers frequency standards and their associated equipments are installed as frequency standards, which supply reference signals to the VLBI system. Also spare units for important parts such as a sampler, TCU and recorder are prepared because the access to Syowa station is very limited and it is difficult to repair serious damages at the site.

3.4.4. Fringe test before shipping

The domestic fringe test was carried out in September 1997 before shipping in order to confirm feasibility of the observation system to be used in Syowa Station. This test served a test of the MFC for the new geodetic VLBI observation system to be used in Syowa Station as well.

Kashima 26m antenna and Mizusawa 10m antenna were used in the fringe test. The VLBI observation units were installed in Mizusawa 10m antenna and the back-end room with the same configuration to be used in Syowa Station. A hydrogen maser system produced by Anritsu Co. Ltd (Mori et al., 1992, Tsuda et al., 1990) was brought into Mizusawa. It was attached to the vibration-defense unit to protect a hydrogen maser unit from the large vibrations that occur during the transportation to Antarctica. The back-end system of the same type was used also in Kashima in the fringe test. At that time, no trouble was met and the MFC detected fringe both in S and X bands.

After the fringe test, VLBI observation equipments are placed in the fourth floor of Shirase in October 1998. Special care was taken by Shirase crew and JARE39 members for hydrogen masers and associated units.

3.4.5. Construction of the VLBI observation system

In the period of the summer operation, the VLBI system was installed as follows.

1. Hydrogen masers and its associated units were transferred from Shirase via transportation on sea-ice and ground. These instruments were installed in the seismography room (figure 3.7) near the MPA and reference signal supplying system was built up there. Figure 3.8 shows an arrangement summary of the hydrogen masers and its associated equipments in the seismography room. Figure 3.9 shows a summary of the reference signal supplying system in Syowa Station as of February 1999. This work was begun prior to other works because preparatory run of two weeks was necessary for stable operation of the hydrogen masers. Figure 3.10 shows photographs of the hydrogen masers and its associated units.
2. The front-end system was built up in the receiver room of the MPA. Input-output levels among the units used in the front-end system were tuned up following the condition of fringe test. Figure 3.11 shows a summary of the front-end system as of February, 1998 and figure 3.12 shows photographs of the front-end system.
3. The back-end system and the antenna pointing system were installed in the satellite data reception room (figure 3.13). Figure 3.14 shows the back-end system and figure 3.15 shows the antenna pointing system in the satellite data reception room. Figure 3.16 is the back-end system as of February, 1998. The development of the antenna pointing system used in VLBI started in the period of JARE38 wintering. A complete version of this tool (Tamura, 2000) was installed in the PC used for antenna control in January, 1998. After building up the front-end and back-end systems, the final pointing test was carried out. The data of this pointing test was transported to Japan via Internet and antenna axis parameters were determined at NAO, Mizusawa by the least square fitting. Seven components of the axis calibration coefficients determined from this pointing test are shown in table 3.1. Figure 3.17 shows sky distribution of the observed radio sources. Name of radio sources used in this test and a number of scans are shown in table 3.2.
4. Four coaxial cables for transmitting the reference signals from the H-maser frequency standard were newly laid between the seismograph room and the satellite reception room. Figure 3.18 shows the construction route of these cables.

Table 3.1 Seven components of axis-calibration coefficient estimated from the pointing test

Calibration Coefficient of Electric Axis	Unit: degree
Inclination of a vertical axis	0.003144
Direction of inclination	117.8469
Non-orthogonal degree of Az-El axes	-0.001928
Non-orthogonal degree of El axis and beam	-0.001048
Component that proportions to the angle of El axis	-0.0006293
Error of Azimuth starting point	0.009241
Error of Elevation starting point	0.000010

Table 3.2 Names and number of scans of radio source used in the pointing

Names of celestial bodies	Number of scan
NGC6334	6
PMNJ0859-4730	21
PMNJ1115-6115	13
W22	16
Orion A	12
Venus	10
Sagittarius A	16
Total	94

A summary of the final specifications of the Syowa VLBI system is shown in table 3.3. Details regarding the above work are given in the activity report of JARE39 (Jike, 1999) and an operation manual of the Syowa VLBI observation system is given in Jike, 1999.

Table 3.3 Specifications of Syowa 11m antenna.

Item	specification
Diameter	11m
Radome Size	17m
Frequency Bandwidth of X band	7860-8600MHz
Frequency Bandwidth of S band	2200-2320MHz
Tsys, X band	117.5K at 8350MHz
Tsys, S band	69.2K at 2260MHz
Aperture Efficiency, X band	48.2%
Aperture Efficiency, S band	Over 50%
Slew speed, Azimuth	6 degree/s
Slew speed, Elevation	3 degree/s
Frequency Standard	Hydrogen Maser, 2 sets

3.4.6. Problems during the construction

Some problems specific to Syowa Station arose during the construction of the observation system.

Since the signal transmission cables connecting the antenna, the data acquisition terminal and the reference signal supplying room are exposed to outside air directly, the observation data is strongly affected by fluctuation of outside temperature and magnetic field. Especially, we could not prepare means to measure changes of length of the reference cables. Also, cable covering is easy to get degraded due to strong ultraviolet rays.

The hydrogen maser frequency standards and the seismographs share the same room. Usually, the room where the hydrogen masers are installed must be controlled its room temperature as stable as possible by using an air conditioner for supplying stable reference signals. However, if an air conditioner is attached to the seismograph room, vibrations due to the air conditioner inevitably produces noises to the seismographs. Accordingly, in the case of JARE39 experiments, the room temperature was controlled by opening and closing a door without an air conditioner and could not be satisfactorily controlled. Hence, when weather changes rapidly, the room temperature also varies remarkably. At the JARE40 experiment an electric heater was introduced for the room temperature control.

Since absolute humidity is extremely low, a head of a magnetic tape recorder is apt to get dirty. Accordingly, the rate of the recording error during the observation

frequently became high. It gave rise to a serious problem in fringe search.

3.5 Regular observations and their summary

JARE39 VLBI members including the author carried out four experiments in February, May, August and November, 1998. The Kashima 26m antenna partially took part in the February and May experiments, and the Parkes 64m antenna in the whole period of the November experiment. In table 3.4a and 3.4b, the observation specifications are listed and the summary of these experiments is shown in table 3.5.

Table 3.4a Observation Specifications

Bandwidth of a base-band	4MHz
Sampling mode	8Mbit/sec, 1bit sampling
Number of used frequency channels	14
Recording Rate	128Mbit/sec
S-band, number of channels and RF bandwidth	6ch, 2217-2302MHz
X-band, number of channels and RF bandwidth	8ch, 8210-8570MHz

Table 3.4b Frequency Arrangement

V.C. Ch. number	Frequency ID	RF Frequency (MHz)
1	X	8210.99
2	X	8220.99
3	X	8250.99
4	X	8310.99
5	X	8420.99
6	X	8500.99
7	X	8550.99
8	X	8570.99
9	S	2217.99
10	S	2222.99
11	S	2237.99
12	S	2267.99
13	S	2292.99
14	S	2302.99

Table 3.5 Summary of experiments conducted during JARE39

Name	Start epoch (UT)	End epoch (UT)	Number of Observation	Station ID
S98040 & 041	98/Feb/09 08:13	98/Feb/11 08:10	318	Hh,Ho,Ka,Sy
S98131 & 132	98/May/11 08:00	98/May/13 08:01	347	Hh,Ho.Ka,Sy
S98221	98/Aug/09 08:00	98/Aug/11 08:08	337	Hh,Ho,Sy
SYW984	98/Nov/09 08:00	98/Nov/11 08:12	398	Hh,Ho,Pk,Sy

Ho: Hobart 26m, Hh: HartRAO, Sy: Syowa Station, Pk: Parkes, Ka: Kashima 26m

We sent back the data of the February experiment to Japan as soon as the experiment finished. Although the MFC produced the correlation data from the February experiment data, it did not detect fringes in the X band for the baselines including Syowa Station. Also a K4 correlator of Geographic Survey Institute did not detect X band fringes for the Kashima-Syowa baseline. Therefore, we concluded that some trouble had occurred in the X band receiving system in Syowa Station. We investigated several possibilities of causes of the trouble. We suspected the sensitivity of X band receiver and pointing accuracy at first. Then we checked several units of the VLBI system. Summary of the test is described in table 3.6.

Some causes of the trouble were rejected by the success of S band. Unfortunately, we could not identify definitive reasons of the trouble at the site. JARE40 (1998-2000) reported the trouble of rapid rise of the system temperature and the cause was supposed that the room temperature of the receiver room got too low. However, whether the cause of the trouble of the February experiment is the same or not is still unclear.

The most anxious problem in the Syowa Experiment was that we could not confirm the observation quality immediately at the site, since we can access there only once a year. To avoid such problem, we prepared a reproducer system at Syowa Station from JARE40. A part of the raw observation data became possible to be taken into a computer and to be processed at the site immediately. Thus thereafter by selecting channels, data of a few second was transmitted to NIPR via satellite communications. Data of a few seconds will be enough to check the system by fringe test, if we select a

strong radio source. These procedures at Syowa Station were summarized in Jike et al. (1999).

The wintering party of JARE39 returned to Japan at the end of March, 1999, and the Syowa's K4 tapes, in which May, August, November 1998 and February 1999 experiments data were recorded, returned in the middle of April. The data obtained in the JARE39 experiments were sent to the MFC operation office.

Table 3.6 Checked items of the X band observation system. Pointing error was estimated from pointing test data carried out in the wintering. Phase calibrator signals were detected by a GSI correlator and their phasess were stable. Polarization is the same as that of the receiving mode of artificial satellite's signals. The difference of the local clock of Syowa VLBI system from GPS time is smaller than 1 microseconds. TCU was locked to reference signals supplied from the hydrogen maser frequency standard.

Checked term	Summary
Aperture efficiency of X band	40.9%-49.7% by actual measurement
Pointing error	less than 0.01 degree
System temperature in X band	117.5K
Phase Calibrator Signals	no problem
Channel cable connection and local freq.	no problem
Polarization of receiving system	RHCP
Clock offset	no problem
TCU	no problem

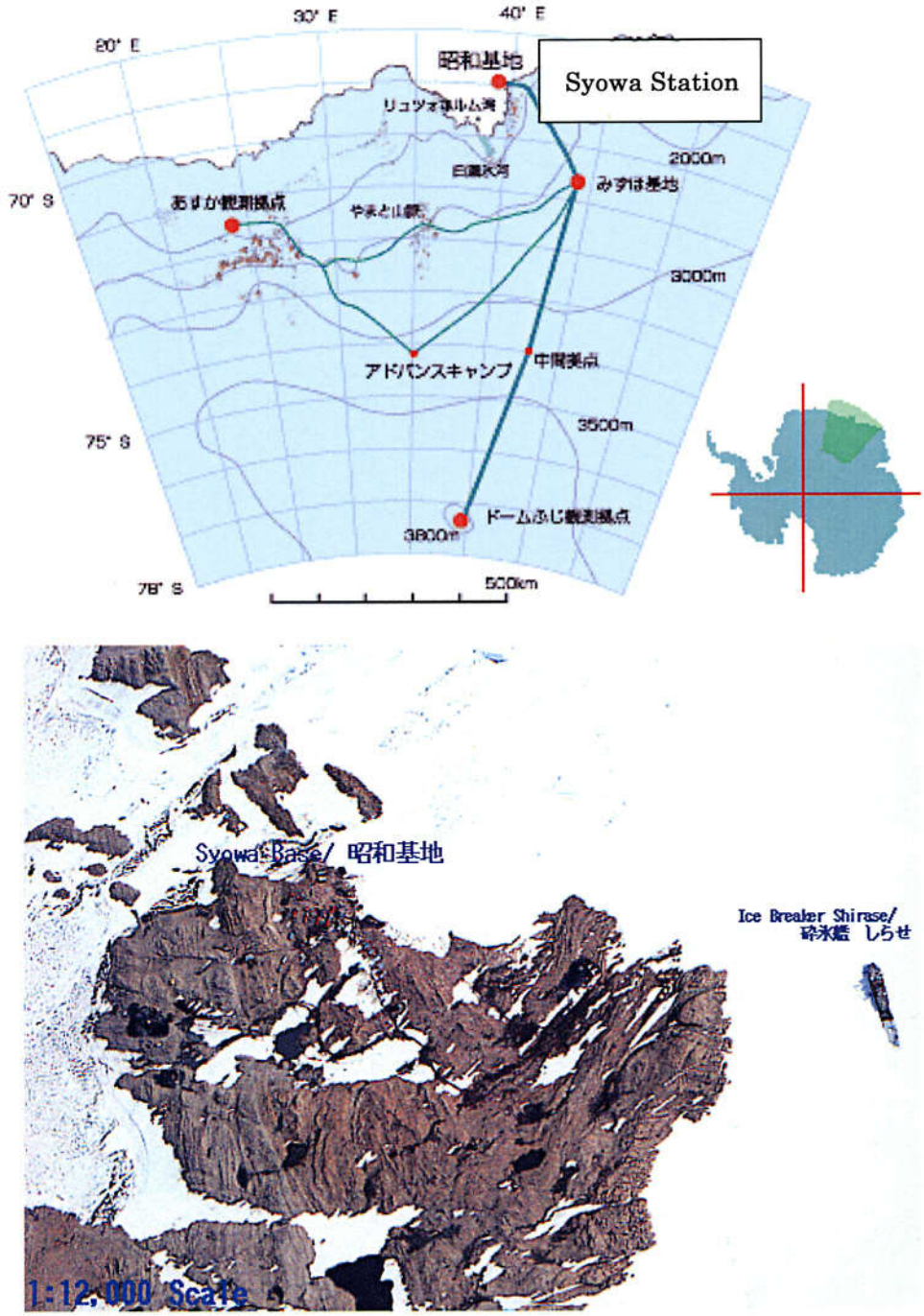

Figure 3.1. Upper: Location of Syowa Station in Antarctica taken from NIPF homepage. Lower: Birds eye view of Ongul Islands (courtesy by GSI).

Figure 3.2 Icebreaker Shirase anchored to the Ongul strait

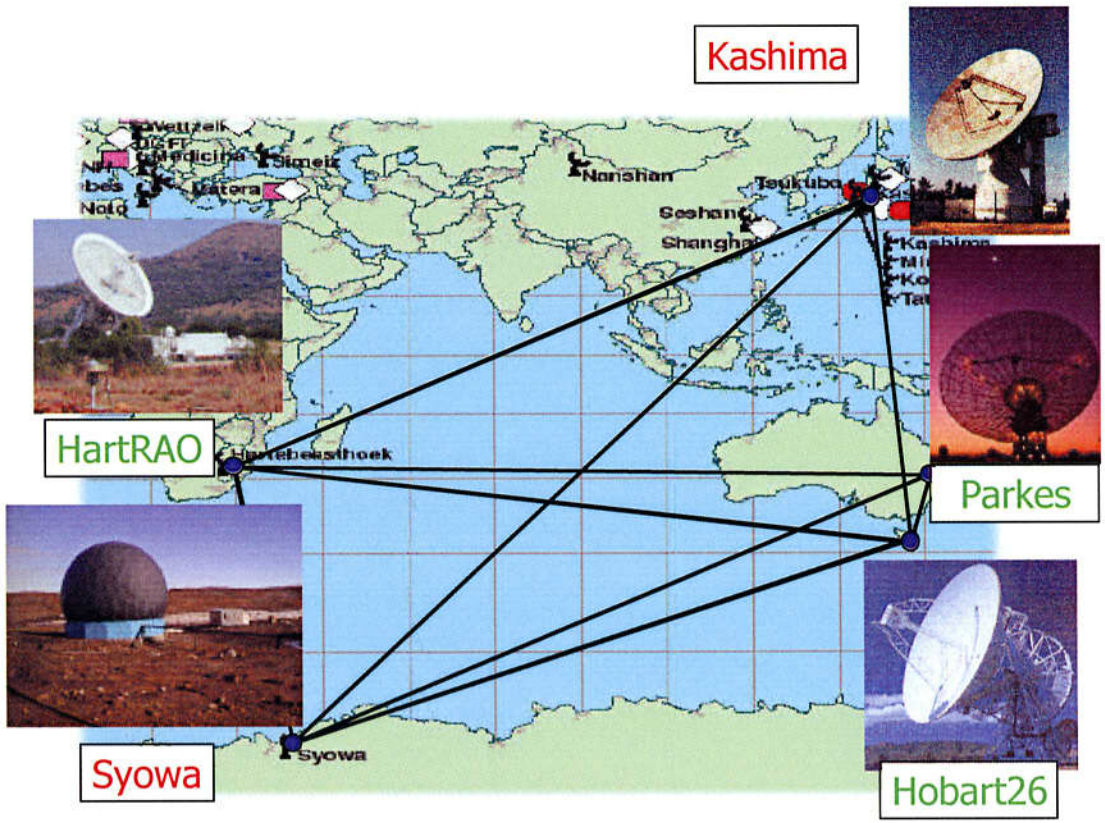

Figure 3.3 Station distribution of the Antarctic VLBI project. The names of S2 stations are shown in green and K4 stations are shown in red. Baseline lengths are 9167618.547m (HartRAO - Hobart26), 9665147.200m (HartRAO – Parkes), 4741786.020m (HartRAO – Syowa), 1089422.043m (Hobart26 – Parkes), 6034892.223m (Hobaer26 – Syowa), 6923086.588m (Parkes – Syowa), 8071140.255m (Hobart26 – Kashima), 11181845.821m (HartRAO – Kashima) and 11391622.605m (Kashima – Syowa).

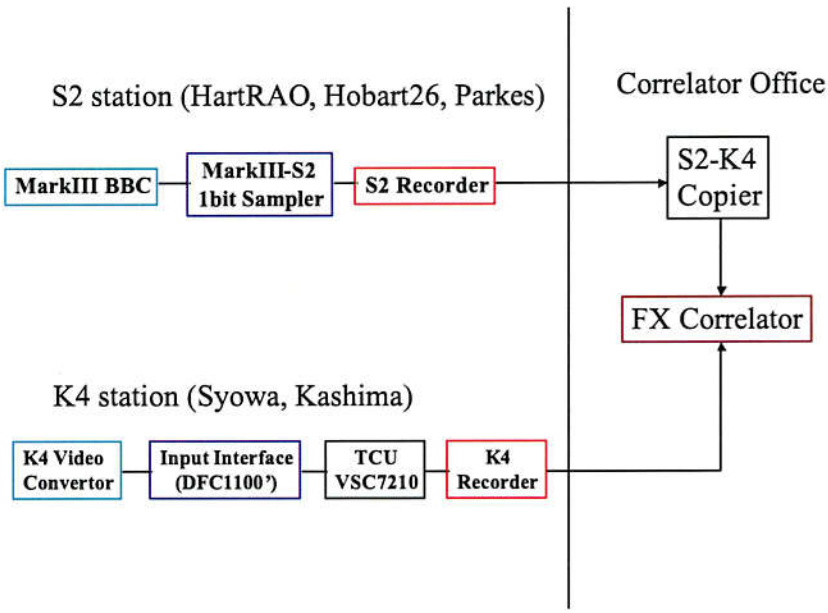

Figure 3.4 Block diagram of the recording systems used in the Antarctic VLBI Experiments. The instruments in the boxes of the same color have almost the same functions. Green: convertor from the intermediate frequency signals to base-band signals separated to individual channels, blue: A/D convertor and formatter, black: unit to add TSS signal and transform data to VSOP format, red: recorder, purple: Correlator.

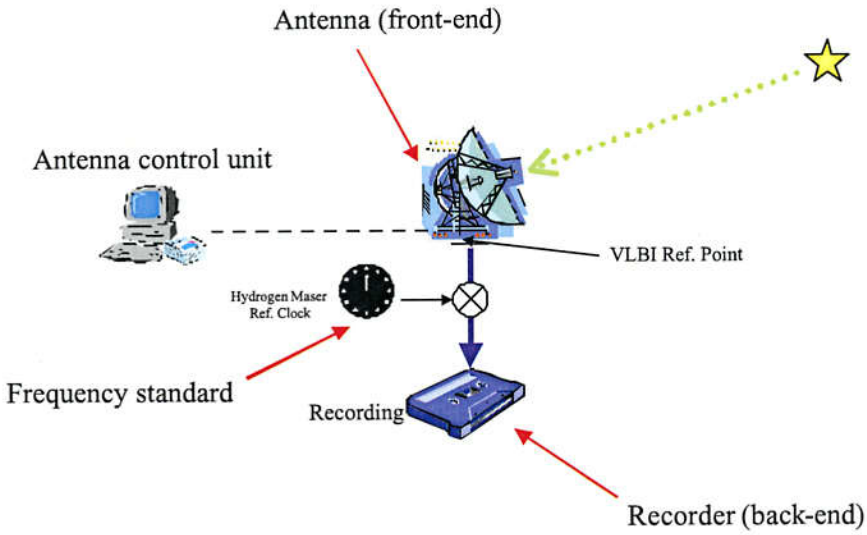

Figure 3.5 Constitution of the VLBI observation system

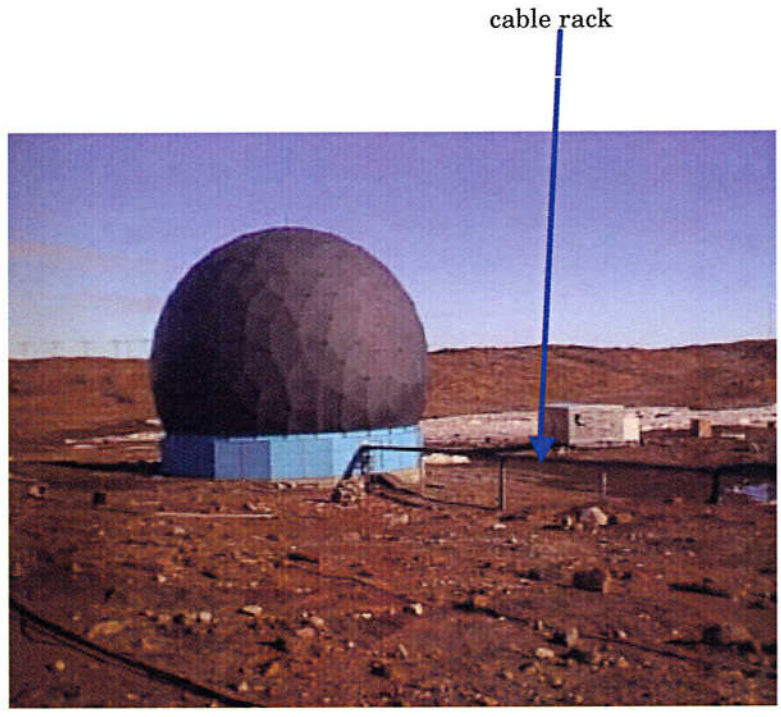

Figure 3.6 The 17m Ra-Dome of the multipurpose 11m antenna in Syowa Station. The structure extending to the right is the cable rack for the Satellite Reception Room. Since there is no soil on the ground and the surface of periphery is composed of the base rock, the cable can not be buried in the underground.

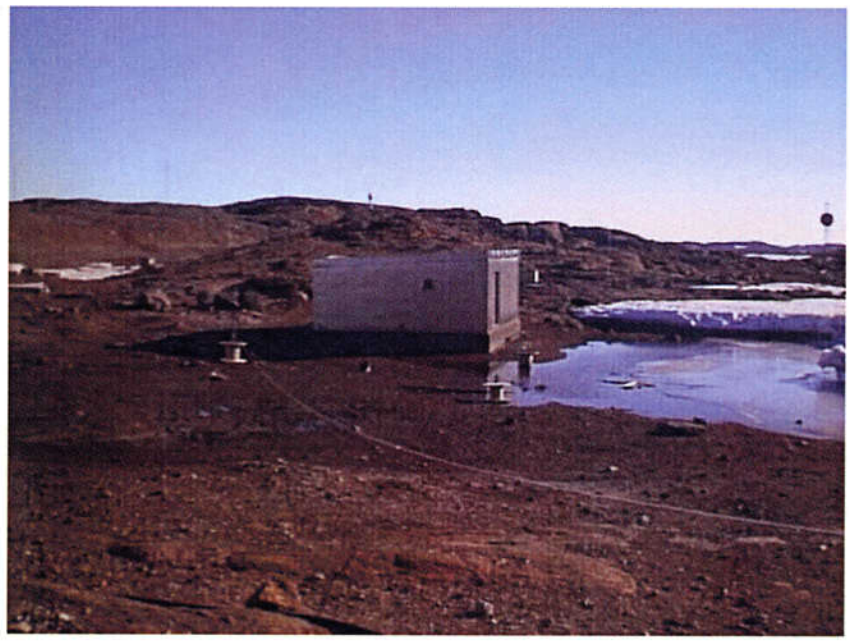

Figure 3.7 The seismograph room where Hydrogen maser frequency standards and associated devices are installed.

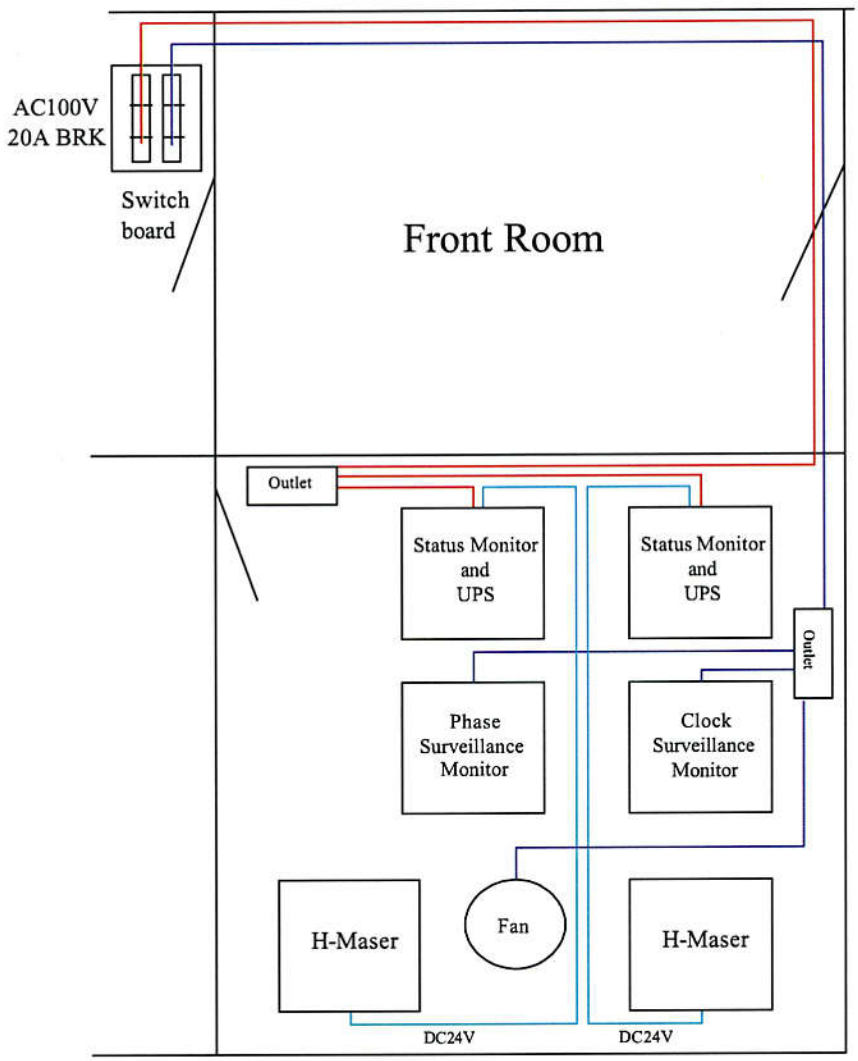

Figure 3.8 Plan view of the seismograph room.

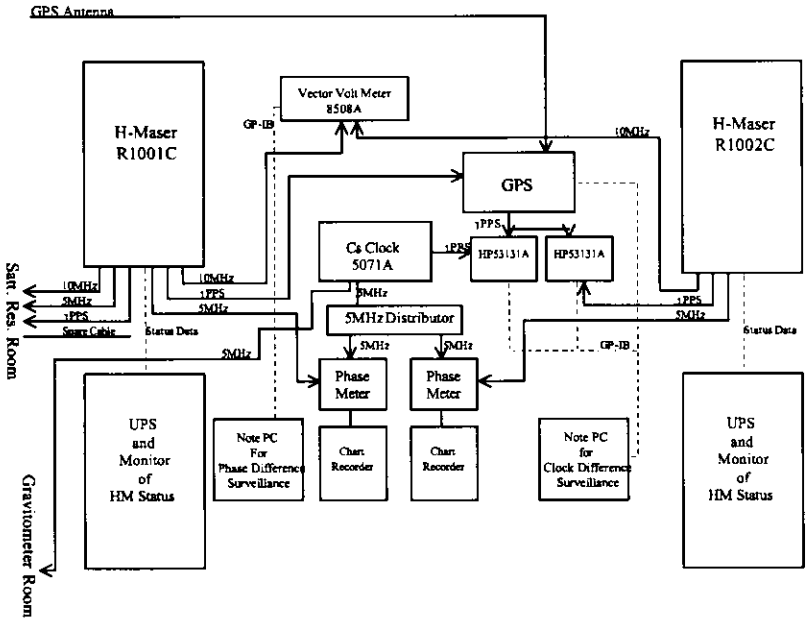

Figure 3.9 Block diagram of the reference signal supplying system in Syowa Station as of February, 1999.

Figure 3.10. The frequency standards. Upper left: main body of the hydrogen maser, upper right: the hydrogen maser status monitor and the UPS, lower left: the phase surveillance monitor, lower right: the clock surveillance monitor.

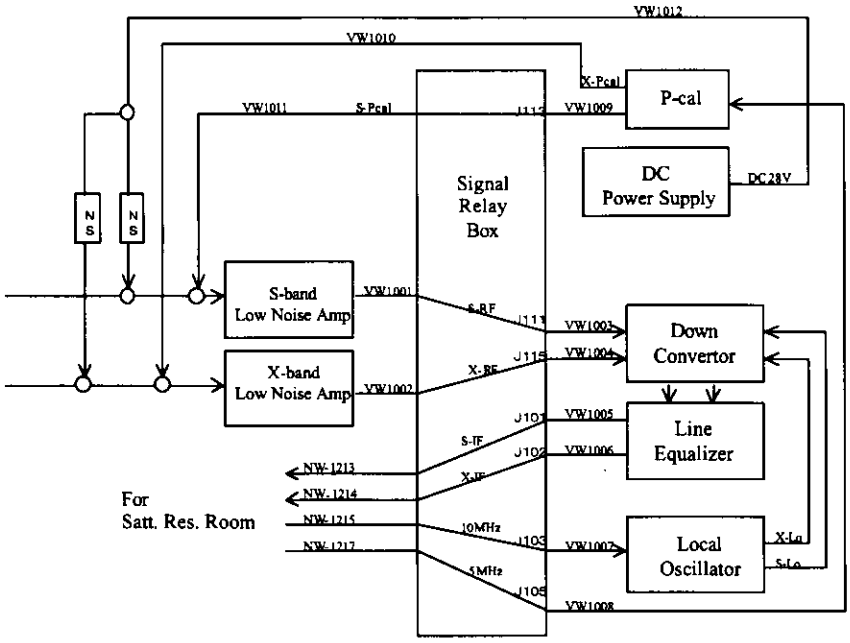

Figure 3.11. Block diagram of the front-end system of Syowa VLBI System as of February 1998

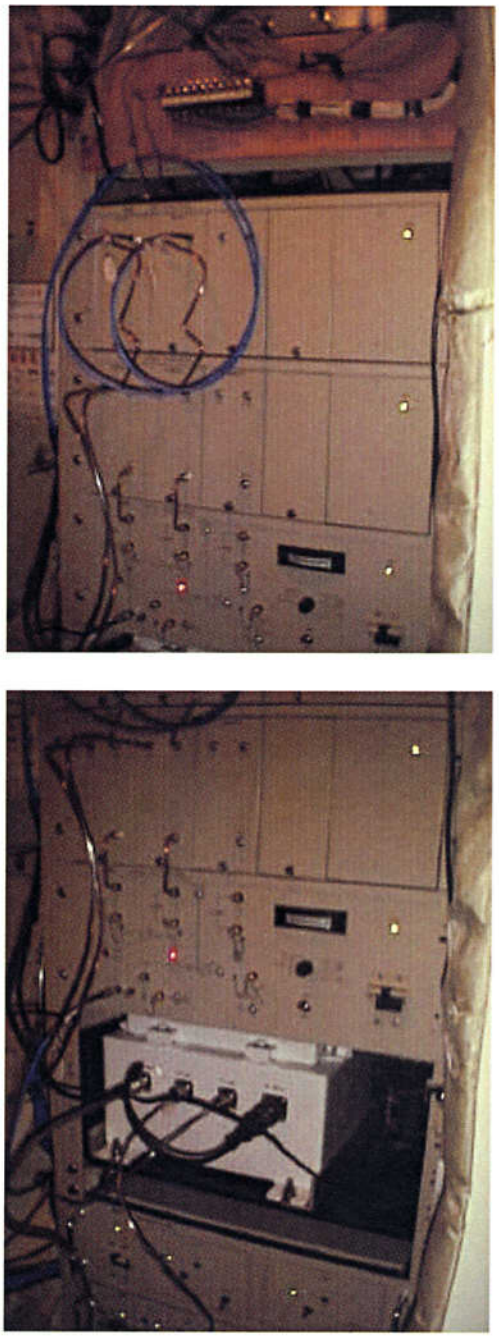

Figure 3.12. The front-end system in the center-hub of the 11m antenna. Upper: down convertor and line equalizer, lower: local oscillator and phase calibrator unit

Figure 3.13 The satellite data reception room where the VLBI back-end system and the antenna pointing system are installed. The signals received by the 11m antenna are terminated in this room.

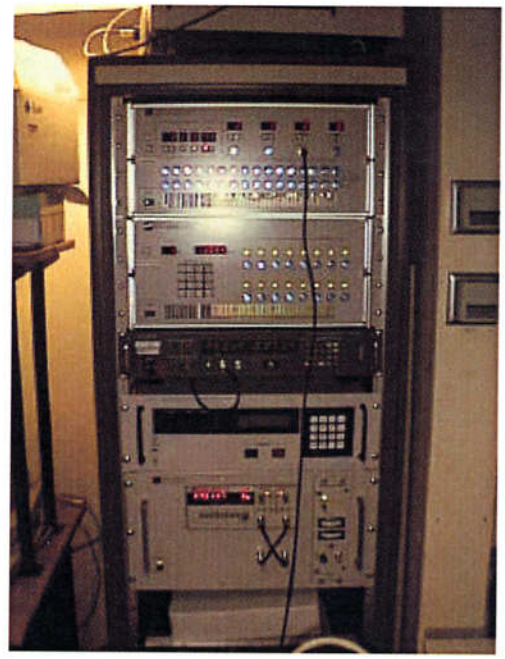

Figure 3.14 The VLBI back-end system in the satellite data reception room. Upper: The K4 terminal, TCU and delay-calibrator. Lower: The recorder, comupter for the field system to control the recorder and the SCSI interface to VLBI raw data.

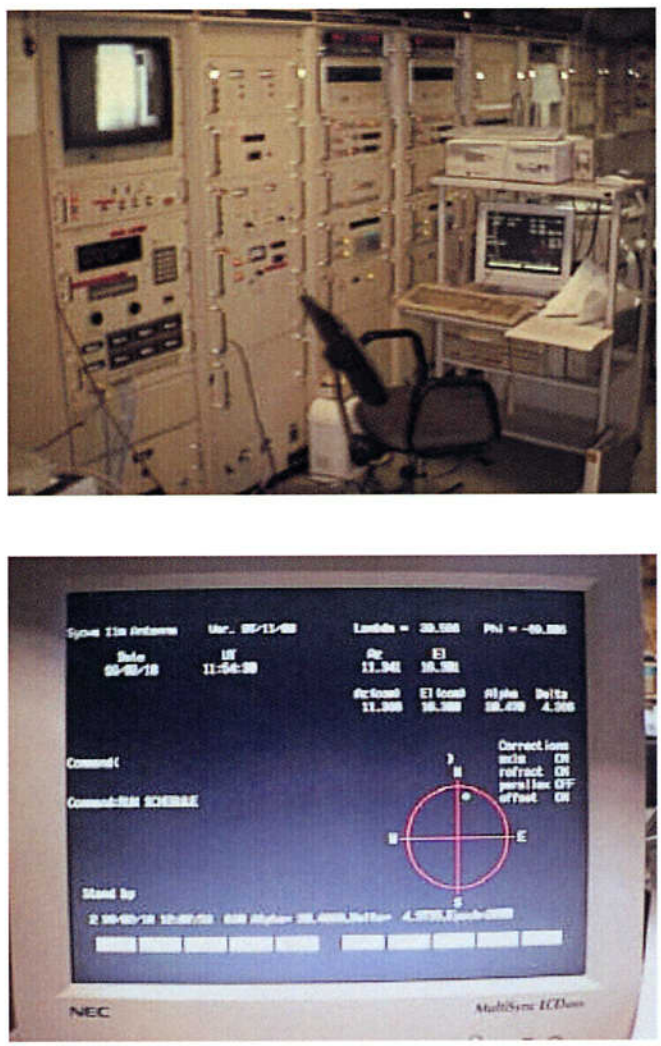

Figure 3.15 The antenna pointing. Upper: panoramic view of the system. Lower: screen shot of the antenna pointing software.

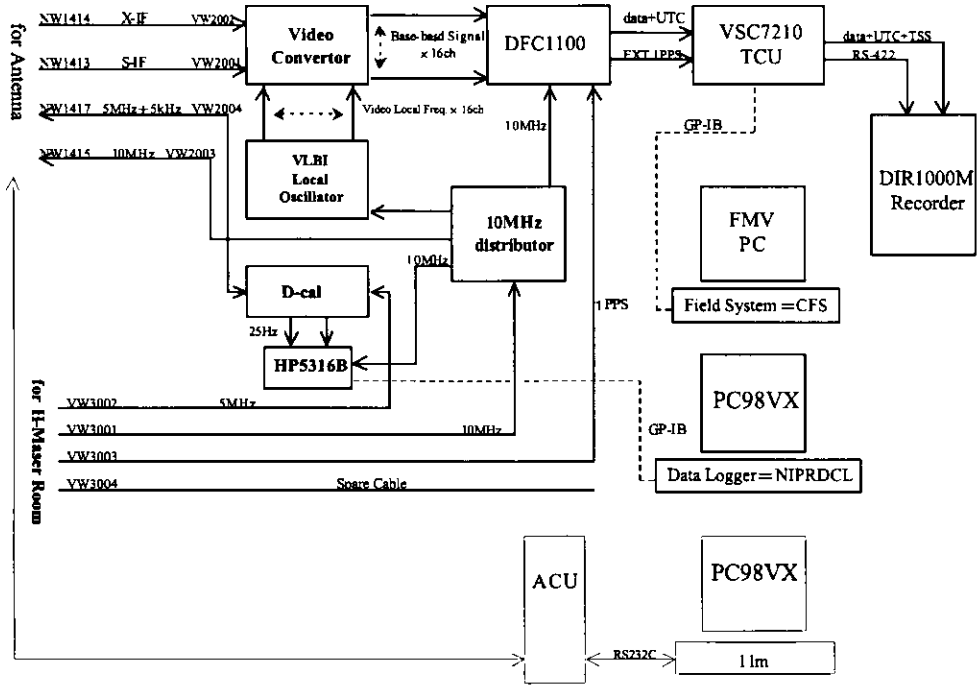

Figure 3.16 The block diagram of the back-end system and the antenna pointing system in Syowa Station as of Ver. Feb. 1998.

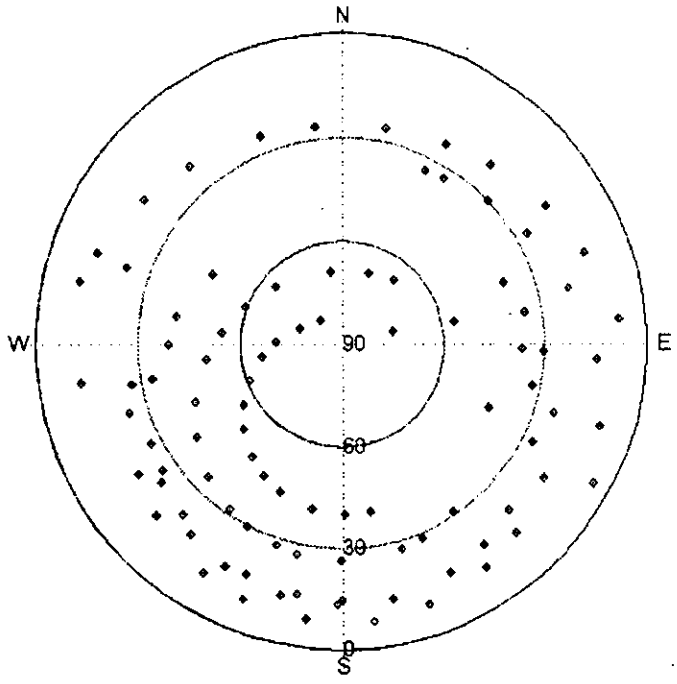

Figure 3.17 Sky distribution of measurements used for the pointing test on February, 1998. It is to be noticed that the distribution is almost uniform.

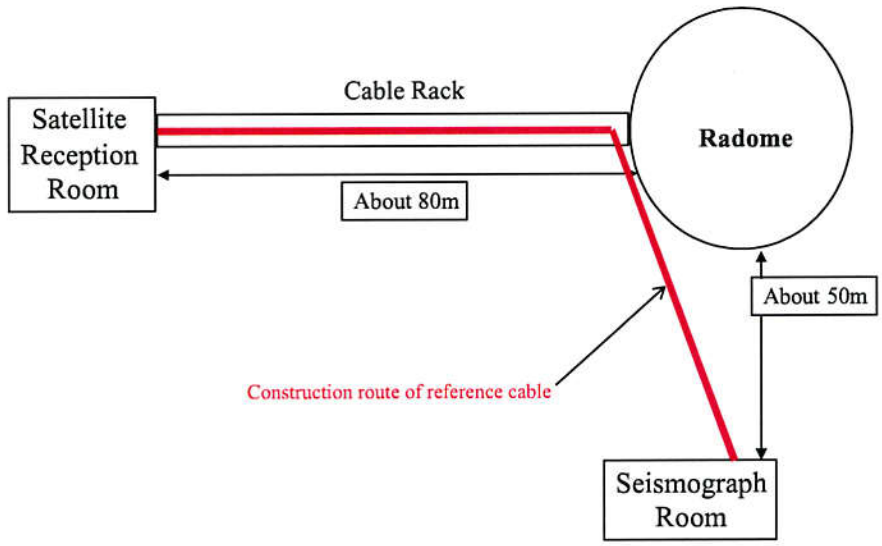

Figure 3.18 The route of four coaxial cables for transmitting the reference signals.

4. Development of the software for the correlation and geodetic analysis

4.1 Introduction

The mixed correlation between K4 and S2 data is a technically unavoidable requirement for the Antarctic VLBI experiment. The Mitaka FX Correlator (MFC) is a unique correlator that can correlate both the K4 and S2 data. However, the correlator had not been used so far for the processing of geodetic VLBI. Moreover, there was no tool for geodetic analysis of the output from the MFC.

In this study, a new analysis system was developed for the MFC and is applied to the Antarctic VLBI data.

The mixed use of K4 and S2 is a consequence of a political situation in the VLBI community rather than academic necessity. In any case, however, we had to resolve this problem to get to geodetic analysis. As a result of developing new software to meet this objective, the position of Syowa Station's VLBI observation point was estimated. This is the first geodetic result obtained from the MFC. Development of this new geodetic analysis system is one of the important outcomes achieved in the Antarctic VLBI project.

Description in this chapter is the summary of the new geodetic analysis system.

4.2 Development of new software

4.2.1. Structure of the newly developed geodetic analysis system

The output data from the MFC is processed in the following procedures.

a) Structure analysis of the correlator output
b) Bandwidth synthesis for precise delay and delay rate determination
c) Addition of environment data such as weather data
d) Time system transformation
e) Determination and removal of delay ambiguity
f) Calculation of the ionospheric delay
g) Database setup
h) Calculation of precise a priori delay and delay-rate
i) Geodetic parameter estimation

The programs corresponding to A through G were newly developed in this study.

Main parts of the development are A, B, D and G. The program CALC3 for procedure H is also improved for incorporating procedure D. The tools A and B are developed for precise determination of delay and delay rate which are used as the observables in the subsequent analyses. The tool D calculates corrections to compensate the difference of the time systems between the correlation processing on the MFC and the tool H. The tool G prepared database files used as a data I/O control system in the tools H and I. Mutual relations among the programs is shown in figure 4.1. Details of the new software and I/O flow are shown in figure 4.2.

4.2.2. Characteristics of processing by the MFC

Before explaining the new geodetic tools, we describe characteristics and data processing of the output from the MFC.

A delay used in VLBI data processing is a time difference of radio wave passages between two VLBI reference points in a celestial reference frame (CRF), as:

$$\tau_g(T_x) = -(\mathbf{Y}(T_y) - \mathbf{X}(T_x)) \cdot \mathbf{s}/c \quad , \tag{4-1}$$

where τ_g is a geometrical delay, **X** and **Y** are position vectors of VLBI stations X and Y, respectively, in CRF, **s** is a direction vector of a reference radio source in CRF, T_x and T_y are epochs when a radio wave passed VLBI stations X and Y, and c is velocity of light in vacuum. The geocenter is adopted as a starting position. T_x is adopted as a reference epoch of the observable, and station X is treated as the time reference station of a baseline.

$X(T_x)$ and $Y(T_y)$ in equation (4-1) are expressed in a terrestrial reference frame (TRF) as:

$$\begin{aligned} \mathbf{X}(T_x) &= \mathbf{P}(T_x)\mathbf{N}(T_x)\mathbf{S}(T_x)\mathbf{W}(T_x)\mathbf{x}(T_x) \\ \mathbf{Y}(T_y) &= \mathbf{P}(T_y)\mathbf{N}(T_y)\mathbf{S}(T_y)\mathbf{W}(T_y)\mathbf{y}(T_y) \end{aligned} \quad , \tag{4-2}$$

where P, N, S and W are rotation matrices of the precession, nutation, diurnal rotation or UT1 and polar motion, and $\mathbf{x}(T_x)$ and $\mathbf{y}(T_y)$ are position vectors of VLBI stations at T_x and T_y in TRF. $x(T_x)$ and $y(T_y)$ are expressed as:

$$\begin{aligned} \mathbf{x}(T_x) &= \mathbf{x}(T_0) + d\mathbf{x}(T_x, T_0) \\ \mathbf{y}(T_y) &= \mathbf{y}(T_0) + d\mathbf{y}(T_y, T_0) \end{aligned} \quad , \tag{4-3}$$

where T_0 is the reference epoch of TRF, dx and dy are displacement vectors of station X

between T_x and T_0 and those of station Y between T_y and T_0, respectively. Geophysical contributions to dx and dy are the crustal movements due mainly to plate motions, the earth tidal deformation, the ocean loading effect, the pole tidal deformation and the atmospheric loading effect and so on at each station.

The VLBI observable includes several contributions besides a geometrical delay. The observable including these contributions is expressed as:

$$t(T_x) = t_g(T_x) + t_{atmy}(T_y) - t_{atmx}(T_x) + t_{ion}(T_x) + t_{clky}(T_y) - t_{clkx}(T_x), \qquad (4\text{-}4)$$

where τ_{atm} is a tropospheric delay, τ_{ion} is an ionospheric delay and τ_{clk} is a clock offset. These are estimated simultaneously with geodetic parameters. In usual analysis of geodetic VLBI, the tropospheric delay and the clock offset are estimated at individual station, and the geometrical delay and the ionospheric delay is obtained from the difference of observed delays in X and S bands.

4.2.2.1 Definition of delay used by the MFC

In processing by the MFC, a delay is defined in "station-based delay system". This delay system adopts the geocenter as a fictional time reference station. A delay is defined as a difference of epochs when the same wave front radiated from a celestial body passes the geocenter and a ground station. This delay is called "station-based delay" and is used as an a priori delay in fringe tracking.

The delays of individual stations X and Y are expressed as:

$$\begin{aligned} t_x(T_g) &= -\mathbf{X}(T_x)\cdot\mathbf{s}/c + t_{pclx}(T_x) \\ t_y(T_g) &= -\mathbf{Y}(T_y)\cdot\mathbf{s}/c + t_{pcly}(T_y) \end{aligned}, \qquad (4\text{-}5)$$

where τ_x and τ_y are station-based delays of X and Y stations, T_g is the epoch when the wave front reaches geocenter and τ_{pcl} is the peculiar delay specific to each VLBI station. These delays are expressed by using the epochs when the wave front arrives at VLBI stations and geocenter as:

$$\begin{aligned} \tau_x(T_g) &= T_x - T_g \\ \tau_y(T_g) &= T_y - T_g \end{aligned}. \qquad (4\text{-}6)$$

A delay between two ground stations is expressed as a difference of the delays between the geocenter and individual ground stations. The delay in the station-based delay system between X and Y station on the ground is expressed as:

$$\tau(T_g) = \tau_y(T_g) - \tau_x(T_g) \quad . \tag{4-7}$$

Substituting equation (4-5) into the equation (4.7), we get

$$\tau(T_g) = -(\mathbf{Y}(T_y) - \mathbf{X}(T_x)) \cdot \mathbf{s}/c + \tau_{cply}(T_y) - \tau_{cplx}(T_x) \quad . \tag{4-8}$$

Although the first term of the right hand side is the same as equation (4-1), it is to be noted that the time argument in the left hand side is different.

4.2.2.2 Characteristics of the output from the Mitaka FX Correlator

There are two types of correlators. One is an XF type and another is an FX type. Output data from an XF type correlator are cross correlation functions. Cross spectra are equal to Fourier transformed cross correlation functions. On the other hand, an FX type correlator outputs cross spectrum directly. The MFC is an FX type correlator.

The MFC adds *a priori* delay to signal at first and transforms to spectrum by using Fourier transform. In this case, phases of the Fourier transforms $x(\omega)$ and $y(\omega)$ of RF signals $x(t)$ and $y(t)$, respectively, are shifted by multiplying $\exp(-i\omega_x\tau_x(T_g))$ and $\exp(-i\omega y\tau_y(T_g))$ to yield the station-based delay spectra given by

$$X(\omega) = x(\omega)\exp(-i\omega_x\tau_x(T_g))$$

and

$$Y(\omega) = y(\omega)\exp(-i\omega_y\tau_y(T_g)), \tag{4-9}$$

where ω_x, and ω_y are RF frequencies of X and Y stations, respectively. The cross spectrum $S_{xy}(\omega)$ obtained from $X(\omega)$ and $Y(\omega)$ is expressed as $S_{xy}(\omega) = X(\omega)Y^*(\omega)$.

If $x(\omega)$ and $y(\omega)$ are expressed as:

$$\begin{aligned} x(\omega) &= \mu_x|a(\omega)|\exp(-i\theta(\omega)) \\ y(\omega) &= \mu_y|a(\omega)|\exp(-i\theta(\omega)) \end{aligned} \quad , \tag{4-10}$$

the cross spectrum $S_{xy}(\omega)$ is transformed to

$$Sxy(\omega) = \mu_x\mu_y|a(\omega)|^2 \exp(-i\omega(\tau_y(T_g) - \tau_x(T_g))) \quad , \qquad (4\text{-}11)$$

where μ_x and μ_y are sensitivities of the antennas X and Y, $a(\omega)$ is the original spectrum radiated by a radio source at frequency ω and $\theta(\omega)$ is a phase of signal at frequency ω. The form of the cross spectrum is the same as the Fourier transformed cross correlation function which is the standard output of an XF type correlator.

Incidentally, a fringe phase ϕ is obtained from a difference between two phase delays of equation (4-7) as:

$$\phi(T_g) = \omega(\tau_y(T_g) - \tau_x(T_g)) , \qquad (4\text{-}12)$$

and it corresponds to a phase of the cross spectrum given by equation (4-11). A group delay is expressed as:

$$\frac{\partial\phi}{\partial\omega} = \tau_y(T_g) - \tau_x(T_g) . \qquad (4\text{-}13)$$

A fringe frequency and a delay rate are expressed as time derivatives of equations (4-12) and (4-13).

In the actual processing, the signal is divided into many short periods (parameter period: PP) and predicted delays are added to each data in a PP. The length of PP is a unit integration time of the correlation processing. In the time length of a PP, it is considered that coherency is kept among the data of each station. As long as this condition is realized, the Fourier transformation, the integration and product arithmetic are carried out. Such processing is repeated while updating a delay prediction polynomial. In addition, FFT is used to perform the Fourier transformation. Therefore, the cross spectrum, which is the output from the MFC, is expressed as the integrated value at every start time of PP and is discrete as $S_{xy}(j,k,n)$, where j (j=1,J), k (k=1,K) and n (n=1,N) are the IF (intermediate frequency) channel, BBC and PP indices, respectively. The unit integration time is a few seconds in the processing of VLBI carried out on the Earth.

The MFC provides the correlated data in the form of FITS (Flexible Image Transport System) which is optimized for astrophysical imaging. However, the structure of FITS

is not suited to geodetic analysis. Therefore, various steps are necessary before starting geodetic analyses. The purpose of the program A is to extract data, which is necessary in the bandwidth synthesis, of every one scan and of one base line from the correlator output. The extracted data corresponds to an observed data-unit reduced by the bandwidth synthesis.

4.2.3. Bandwidth synthesis

A cross spectrum is separated to a signal component from a radio source and a thermal noise component from receiving units. Usually, the signal is weaker than noise and hardly detectable in each PP except for an observation of a particularly strong radio sources. Noises gradually become smaller with averaging. Accordingly, by the integration of the cross spectrums along the frequency direction and PP direction, it is able to obtain the cross spectrum at arbitrary frequency with high accuracy. Bandwidth synthesis searches a maximum absolute value of the cross spectrum using the relation between the group delay and frequency given by equation (4-13)

Since an observable used in usual geodetic analysis is not the phase delay but the group delay, it is necessary to use the data covering a wide frequency range in order to obtain accurate group delay from the differentiation give by equation (4-13). The bandwidth synthesis is a commonly used technique to realize effectively wide range of receiving frequency. In this technique, the down-converted signal is sampled in several base band channels separated with appropriate intervals. The bandwidth synthesis integrates the cross spectrum between the channels.

In the bandwidth synthesis for precise delay determination, the cross spectrums $S_{xy}(j,k,n)$ are integrated as:

$$F(\Delta\tau,\Delta\dot{\tau}) = \frac{1}{N}\sum_{n=1}^{N}\{\frac{1}{K}\sum_{k=1}^{K}[\frac{1}{J}\sum_{j=1}^{J}S_{xy}(j,k,n)\exp(-i\omega_{vj}\Delta\tau)]\exp(i\Phi_k)\}\exp(-i\omega_{0k}\Delta\dot{\tau}n\Delta t). \quad (4\text{-}14)$$

Here, following notations are used.

ω_{vj} : frequency of the j-th IF frequency channel
Φ_k : P-cal phase of the k-th base band channel
ω_{0k} : RF frequency of the k-th base band channel
$\Delta\tau$: delay revision
$\Delta\dot{\tau}$: delay rate revision
Δt : time length of a PP .

$\Delta\tau$ and $\Delta\dot{\tau}$ such that

$$\left|F(\Delta\tau,\Delta\dot{\tau})\right| = \text{maximum} \qquad (4\text{-}15)$$

are adopted as solutions of the bandwidth synthesis. In developing this program, previous works (Kondo 1982, Kawaguchi and Kawano 1984, Takahashi et al., 1997) were referred to. Although the main logic of this program is almost the same as those described in these works, this new program enables us to avoid ill-convergence problem in finding a maximum by calculating the delay with finer resolution in comparison with the past reports and by adopting subplex method.

A priori delay produced by the MFC is given with respect to the geocentric time system and hence the group delay obtained with the bandwidth synthesis is necessarily given in this system.

Characteristics of the bandwidth synthesis thus developed are as follows.

a) The transformation from the cross correlation function to cross spectrum is omitted.
b) The solution is expressed with the group delay that is referenced to the geocentric time system.
c) The phase equalization between BBC's is carried out for individual PP's to handle the rapid phase fluctuation of the phase calibrator.
d) Delay search processing of each scan is carried out in three steps. The first two steps are a single band delay search and a multi band delay search. In these steps, delay search window is made as narrow as possible to find the final solution in the third step by a fine search.

The station-based delay system is different from the delay system used in the usual geodetic analysis. Consequently, the solutions of the bandwidth synthesis are not directly usable in the software for the subsequent geodetic analysis (steps H and I in 4.2.2), namely, CALC3 and MSLV. Hence, further modification of the data is required.

4.2.4. Time system transformation

As mentioned above, the solution of the bandwidth synthesis is expressed in the geocentric time system, while the usual geodetic analysis is based on the baseline time system. The delay in the baseline time system $t_B(T_x)$ is expressed as:

$$\tau_B(T_x) = -(\mathbf{Y}(T_y) - \mathbf{X}(T_x)) \cdot \mathbf{s}/c + \tau_{other} \qquad (4\text{-}16)$$

and the delay in the geocentric time system $t_G(T_g)$ is expressed as:

$$\tau_G(T_g) = -\mathbf{Y}(T_y) \cdot \mathbf{s}/c + \tau_{cply}(T_y) - (-\mathbf{X}(Tx) \cdot \mathbf{s}/c + \tau_{cplx}(T_x)), \qquad (4\text{-}17)$$

where

$$\tau_{other} = (\tau_{atmy}(T_y) - \tau_{atmx}(T_x)) + \tau_{ion}(T_x) + (\tau_{clky}(T_y) - \tau_{clkx}(T_x)) \qquad (4\text{-}18)$$

and

$$\tau_{cply}(T_y) - \tau_{cplx}(T_x) = -(\tau_{atmy}(T_y) - \tau_{atmx}(T_x)) - \tau_{ion}(T_x) + (\tau_{clky}(T_y) - \tau_{clkx}(T_x)) \ . \qquad (4\text{-}19)$$

The time system transformation is the process to transform the delay in the geocentric time system to the one in the baseline time system. There are two processes in this time system transformation. One is to calculate a difference of delays between the two time systems and the other is the shift of the reference clock station.

In the case that the two delays refer to the same wave front, the difference of the delays given by equations (4-16) and (4-17) is a correction associated with the time system transformation. The difference between equations (4-16) and (4-17) is shown as:

$$\Delta\tau_{tst} \equiv \tau_B(T_x) - \tau_G(T_g) = \tau_{other} - (\tau_{cply}(T_y) - \tau_{cplx}(T_x)) \qquad (4\text{-}20)$$

Rigorously speaking, the first two terms of equation (4-20) do not agree with the third term because the clock rate at the geocenter differs from the one on the ground due to the difference of the gravity. However, this general relativistic effect in the time system transformation under concern is extremely small and disregarded here.

As seen in equation (4-19), in the station-based delay, the effect of the atmospheric propagation delay appears as if it were negative, and hence, the total delay is shorter than the geometrical delay. Substituting equations (4-18) and (4-19) into the right hand side of equation (4-20), equation (4-20) is finally expressed as:

$$\Delta\tau_{tst} = 2(\tau_{atmy}(T_y) - \tau_{atmx}(T_x)) + 2\tau_{ion}(T_x) \quad . \qquad (4\text{-}21)$$

Next, we describe the change of a reference clock station from the geocenter to a ground station X. Suppose that the observed wave front that passed the geocenter at T_g

passes the ground station X at T_x. Then, the time difference between two reference clock stations corresponds to the station-based delay at X station in the geocentric time system. The relation of the two epochs T_g and T_x is expressed by the following equation as:

$$T_x = T_g - \mathbf{X}(T_x)\cdot \mathbf{s}/c + \tau_{cplx}(T_x) \quad . \tag{4-22}$$

This relation is illustrated in figure 4.1. The magnitude of the delay correction by this process is of the order of 1~10 nanoseconds.

From equations (4-21) and (4-22), $\tau_B(T_x)$ is expressed as:

$$\tau_B(T_x) = \tau_B(T_g - \mathbf{X}(T_x)\cdot \mathbf{s}/c + \tau_{cplx}(T_x)) = \tau_G(T_g) + \Delta\tau_{st} \quad . \tag{4-23}$$

This is the final form of the baseline-based delay after the time system transformation.

Eventually, the solution of the bandwidth synthesis is defined as:

$$\Delta\tau_{BWS}(T_g) = \tau_B(T_x) + \tau_{rsd}(T_x) - \tau_G(T_g) \tag{4-24}$$

where $t_{rsd}(Tx)$ is the residual delay at T_x. t_{rsd} is equal to the difference between the observed delay and predicted delay in the baseline-based delay system. The total delay is expressed as $t_B(T_x) + t_{rsd}(T_x)$. By the time system transformation, the solution of the bandwidth synthesis is changed to:

$$\Delta\tau_{BWS}(T_g) = \Delta\tau_{tst} + \tau_{rsd}(T_x) \quad . \tag{4-25}$$

Accordingly, twice the atmosphere propagation delay is added to the solution of the bandwidth synthesis as given by equation (4-21). This is a notable difference between the two time systems. Figure 4.2 explains the difference of the two delays from the prediction.

The data reduction usually uses the residual delays. To extract $\tau_{rsd}(T_x)$ from the solution of the bandwidth synthesis, the time system transformation tool calculates the station-based delay of station X at T_x and the atmosphere propagation delays at stations X and Y at T_x and T_y, respectively. The software named CALC3, which calculates theoretical delays and delay-rates for geodetic analysis, is modified to incorporate the time system transformation. By these processing, comparison of observed delay obtained from the MFC and a priori delay computed with CALC3 becomes possible.

The reference time system used for observations is UTC or TAI. The time rate at the geocenter differs from one on the earth's surface. The time system transformation between UTC and TDB follows those given in IERS Technical Note 21(McCarthy, 1996)

Original results of the bandwidth synthesis are shown in figure 4.3, which are expressed in the geocentric time system. Also, results of the time transformation is shown in figure 4.4 In figure 4.4, delays are expressed in the baseline time system, which is used in usual geodetic VLBI analyses. It is able to confirm that scattering of delay residual is converging at about 1/100 by comparing between figure 4.3 and figure 4.4.

4.2.5. Summary of the newly developed software

Figure 4.5 shows the structure of the new analysis system and figure 4.6 shows details of the new software and the related data I/O. At present, although FITS and its I/O routines are used in the analysis and management of additional data such as weather data and EOP, programs to manage the additional data and also to control the analysis flow are not fully implemented in the new system. Various problems are likely to occur as VLBI data increase without these control programs. Accordingly, construction of the control system is an important task left to complete the VLBI analysis system.

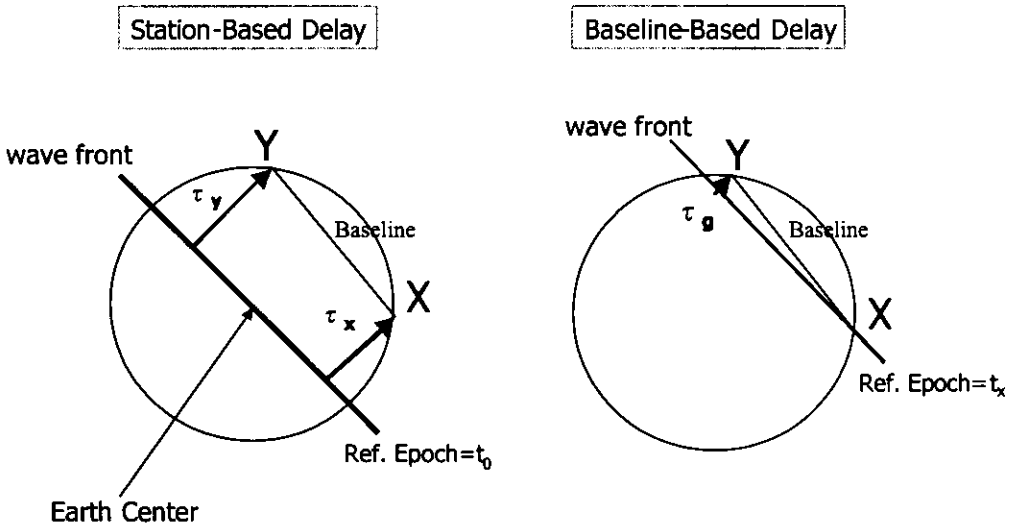

Figure 4.1. Station-based delay and baseline-based delay. Reference epoch of the station-based delay is the time when a wave front reaches the earth center. The delay observable of a baseline is defined as a difference of two station-based delays. In the case of the baseline-based delay, reference epoch is the time when a wave front reaches X station.

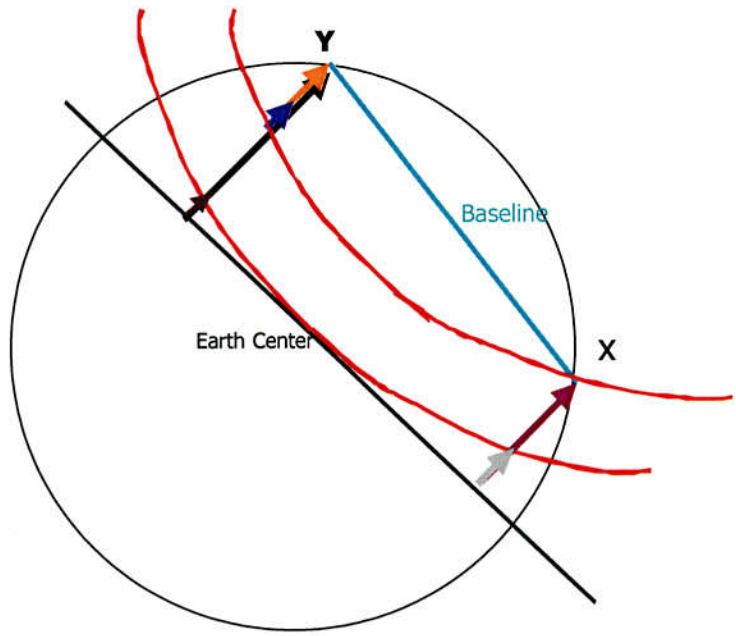

Figure 4.2 Wave fronts affected by the atmospheric delay.
The two red curves express the wave front distorted by the atmospheric propagation delay. The arrows of different colors distinguish various delays such follows.
purple(A): the geometrical delay of station X in the station-based system,
black(B): the geometrical delay of station Y in the station-based system,
ash(C): the atmospheric propagation delay at station X in the station-based system,
brown(D) the atmospheric propagation delay at station Y in the station-based system,
yellow(E): the geometrical delay in the baseline-based system,
blue(F): the atmospheric propagation delay in the baseline-based delay.
Predicted baseline-based delay is given by E+F. Predicted station-based delay of X station is given by B-D. Predicted station-based delay of Y station is given by A-C.

If the same wave fronts are observed, the difference between the station-based delay and the baseline-based delay is expressed as E+F-{(A-C)-(B-D)}. It is supposed that the speed of the radio wave in the earth is the same as the speed in the vacuous. This is justified, since the station at the geocenter is fictition and introduced only for computational ease. Furthermore, C-D is almost equal to F.

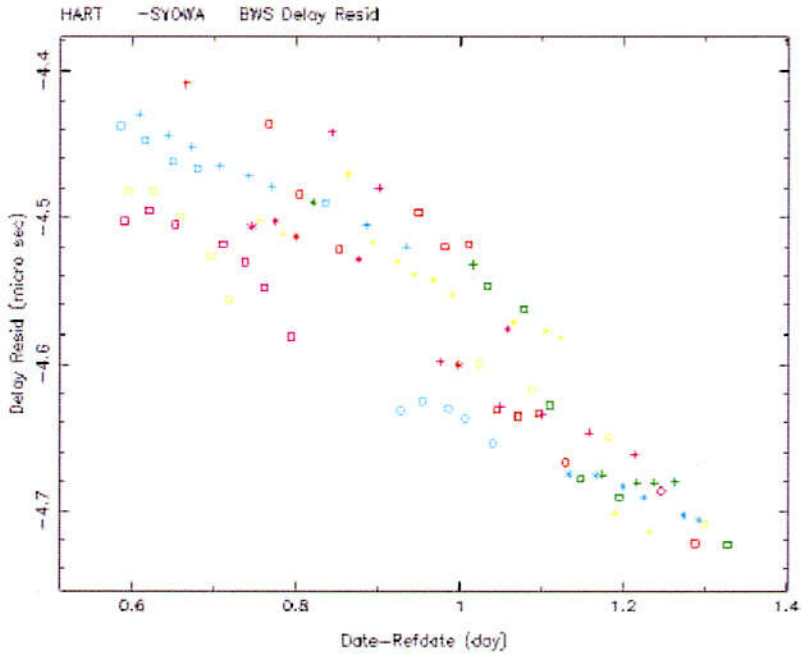

Figure 4.3. Original result of the bandwidth synthesis in chronological order. These delays are taken from the data processing of X band, HartRAO – Syowa baseline, SYW984. X-axis is the progress time (day) from start time of the observation. Y-axis is the delay residual obtained by the bandwidth synthesis and its unit is microsecond. The same mark is used every radio source.

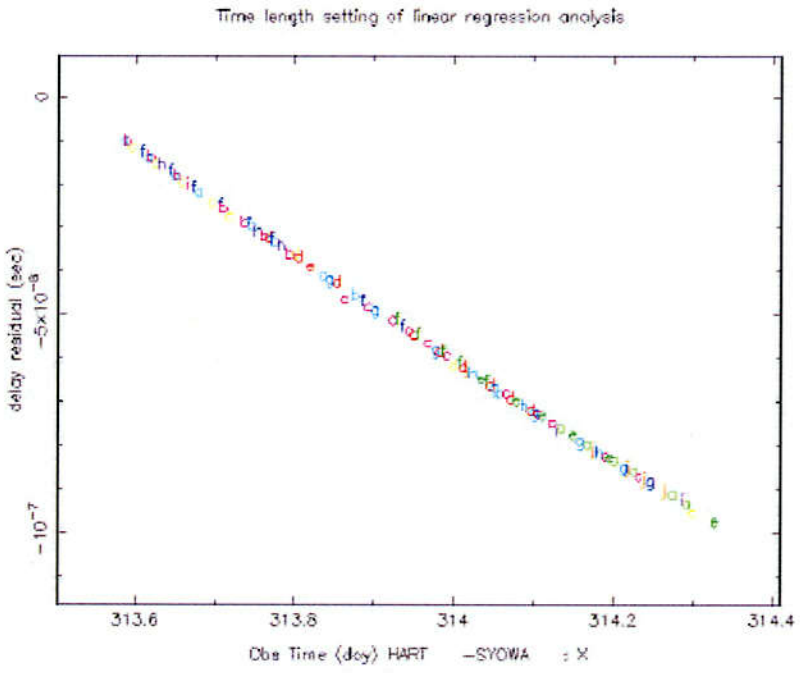

Figure 4.4. The delays after the time system transformation. Attribute of data is same with figure 4.3. X-axis is day of year and its unit is day. Y-axis is delay residual and its unit is second. The cause that the results are arranged to almost straight line is clock offset and clock rate.

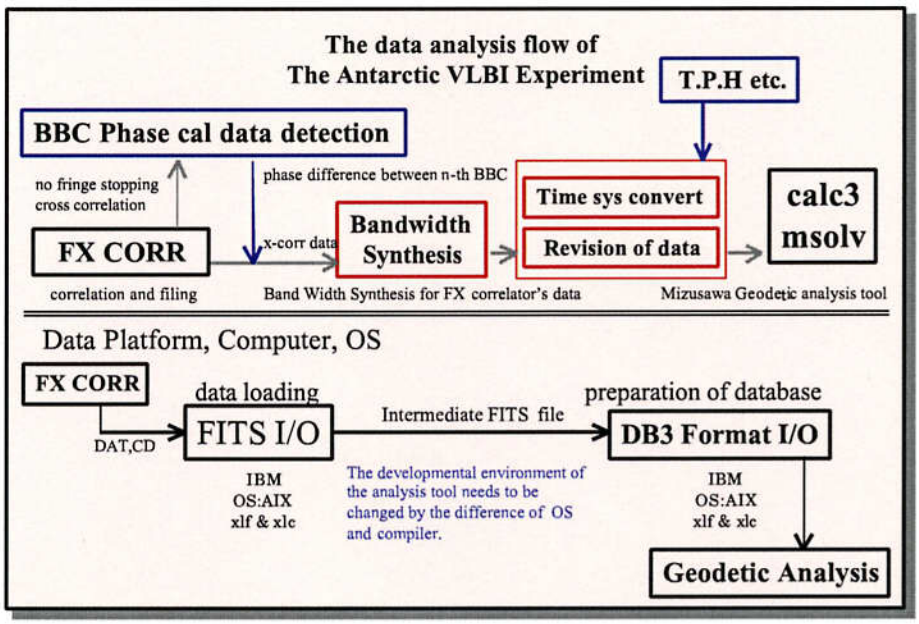

Figure 4.5. Structure of the geodetic analysis system used in the reduction of the Antarctic VLBI Experiment. The blue boxes denote imported data. These red boxes are newly developed software.

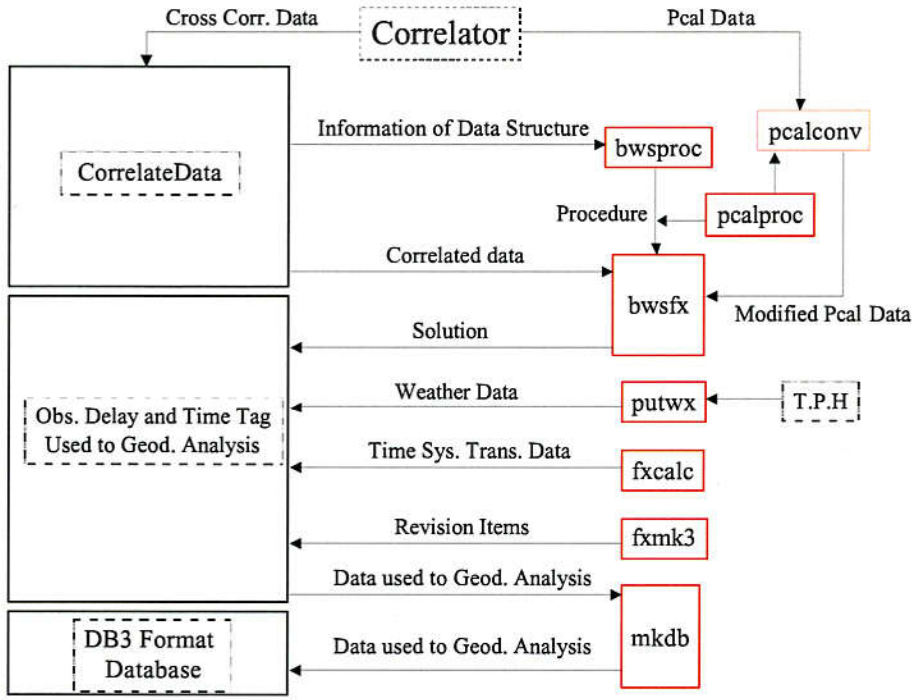

Figure 4.6. Details of new software and related data I/O. The newly developed software is enclosed in a red frame. The arrows show directions of the data flow.

5. Results of analysis and the geodetic interpretation

5.1 Introduction

The geodetic analysis was performed for the data in November, 1998. At first, precise theoretical delays are calculated by CALC3. Then, geodetic parameters are estimated by MSOLV by using the previously computed precise theoretical delays and observed delays determined as in the previous chapter. In these processes, the input and output of the data is controlled in the database DB3.

5.2 Summary of correlation processing

The correlation processing of the data obtained with the Syowa experiment in 1998 by the MFC started soon after the arrival of the data to Japan in April 1999.

The data of the November experiment was correlated first because we considered that possible operational problems would have been best solved in this experiment. In fact, fringes were detected for all baselines.

However, in other experiment, some troubles were occurred and we could not get fringes enough for geodetic analysis. About the failure of the February experiment, its causes were already described in section 3.5. In the May experiment, the fringe amplitude decreased gradually as the observation went on. It is inferred that the head of the recorder had gradually got dirty. No fringe was detected for all baselines in the August experiment unfortunately and its cause is still unclear.

The summary of the correlation processing is shown in table 5.1. Usable results were obtained only in the November experiment.

At the beginning of the correlation processing, the MFC could not detect phase calibration signals, but this problem was overcome by the cross-correlation without fringe rotation.

Table 5.1 Results of the correlation of Syowa Experiment conducted by JARE39

Baseline	JA98040	JA98041	JA98131	JA98132	JA98221	SYW984
Hh-Ho	○	○	-	○	×	○
Hh-Sy	S	S	○	×	×	○
Hh-Ka	○	-	-	○	-	-
Hh-Pk	-	-	-	-	-	○
Ho-Sy	S	S	-	×	×	○
Ho-Ka	○	-	-	○	-	-
Ho-Pk	-	-	-	-	-	○
Sy-Ka	S	-	-	×	-	-
Sy-Pk	-	-	-	-	-	○

○: Fringes were detected in plural scans

×: No fringe wad detected.

S: Fringes were detected from only S band data.

5.3 Results of the analysis

5.3.1. Analysis setting

Geophysical models used in calculating the theoretical delays are as follows.

1. Earth tidal deformation is computed on the basis of Wahr's (Wahr, 1981) love and shida numbers, and the tidal-generating potential (Cartwright and Tayler, 1971; Cartwright and Edden, 1973).
2. Ocean loading displacements are computed by GOTIC2 (Matsumoto et al., 2001) on the basis of the NAO99b ocean tide model (Matsumoto et al., 2000).
3. Atmospheric loading displacements are not taken into account.
4. NHFM2 (Niell, 1996) is adopted as a mapping function of the atmospheric propagation delay.
5. Earth rotation parameters are taken from the IERS Bulletin B.
6. IAU1980 (Wahr, 1981; Seidelman, 1982) is adopted as a nutation model.
7. Station and radio source positions are taken from GLB886 (Ma et al. 1996) and GLB1069 (Ma et al. 1998), respectively.

Furthermore, the ionospheric delay is independently estimated from the difference of observed delays in X and S bands.

Although the accuracy of the adopted nutation model is not enough compared with the present-day accuracy of VLBI, the nutations in longitude and obliquity are estimated in the subsequent step. Therefore, the adoption of the inaccurate nutation model as initial parameters does not affect the final geodetic results. Similarly, since newer and more precise catalogues of station and radio source positions are referred to in the estimation process, the above old catalogues do not cause any problems.

In the next step, following parameters are estimated simultaneously.

1. Position of the Syowa VLBI reference point
2. Zenith atmospheric delay at every one hour at each VLBI station
3. Clock polynomial at each VLBI station
4. Nutation in longitude and obliquity at the mean epoch of the observations

Coordinates and velocities of Hobart, HartRAO and Parkes are substituted by the values given in ITRF2000, and radio source positions are taken from ICRF2000. Although the purpose of this analysis is the estimation of the position of Syowa VLBI reference point, the nutation is also estimated, since the nutation model used to calculate the a priori delays is old and inaccurate and likely to cause biases and large variances of the other estimators. The initial position of stations and radio sources are shown in Appendix A.

Tukey's M-estimation is adopted as a fitting method in order to automatically detect outliers and remove them. Weights of the individual observations are also automatically assigned with this method and the SNR's are not used in the weighting.

5.3.2. Coordinates of the Syowa VLBI reference point

In this estimation, only delays are used. The number of used observations is 364 and total number of adjusted parameters is 83. Standard deviations of delay residuals of individual baselines are shown in table 5.2. Distributions of the delay residuals for the individual baselines are also shown in figure 5.1.

The position of Syowa VLBI reference point in the geocentric Cartesian coordinates at the nominal epoch of November 11, 1998 is estimated to be

$$X= 1766194.143 \quad \sigma_X=0.029\text{m}$$
$$Y= 1460410.932 \quad \sigma_Y=0.025\text{m}$$
$$Z=-5932273.353 \quad \sigma_Z=0.062\text{m}.$$

An error ellipsoid is shown in figure 5.2.

Table 5.2 Standard deviations of the post-fit residual delays for the individual baselines.

Baseline	Standard deviation in sec.
HARTRAO -HOBART26	3.14E-10
HARTRAO -SYOWA	2.45E-10
HOBART26 -SYOWA	3.58E-10
HOBART26 -PARKES	2.79E-10
SYOWA -PARKES	3.45E-10
HARTRAO -PARKES	2.65E-10
AVERAGE	3.02E-10

5.3.3. Discussions on errors

The standard deviation of the vertical component is about three times as large as those of the horizontal components. This does not contradict the error estimation of the VLBI position measurement reported by Takahashi (1994) and Takahashi et al. (1997). The errors are almost of the same magnitude both for the N-S and the E-W components. The reason is that the azimuthal distribution of observed radio sources is almost isotropic (figure 5.3).

However, the standard deviations of the Syowa's positions obtained in this analysis are larger than typical values of recent inter-continental VLBI experiments. In addition standard deviation of the post-fit residuals are 300 ps (pico seconds), which is also much larger than typical values. Causes of errors can be classified into two. One is characterized by a design matrix used in the estimation. The design matrix is determined by network constitution and temporal and spatial distributions of observed radio sources, i.e., observation schedule. The other is characterized by quality of individual observations, i.e., statistical distribution of residuals.

As for the first possibility, the shape of the station network looks good and the observation schedule was made so as to be optimum for the estimation of the position of the Syowa VLBI reference point by using the scheduling software named "SKED" in the auto-scheduling mode. Furthermore, if scattering of the post-fit residuals were as small as those of typical inter-continental experiments, the error estimates of the Syowa's position would have been 1cm or smaller. Hence, it is not likely that the first possibility is the main reason of the large error estimates.

Potential causes of the large scattering of the post-fit residuals are:

1) Inappropriate modeling of the clock and clock rate and the time variation of the zenith atmospheric delay.
2) Thermal noise error
3) Error in the time system transformation
4) Position errors of VLBI stations and radio sources
5) Inaccuracy and/or negligence of the adopted geophysical parameters
6) Other possibilities

1) Inappropriate modeling of the clock behavior and the zenith atmospheric delay

The errors in the clock-offset and the atmospheric propagation delay are included in the observed delay. The clock behavior at each station is modeled by piecewise continuous polylines. Typical timescale of the variation is a few hours. Similarly, the variation of the zenith atmospheric delay are approximated by piecewise continuous polynomials with typical nodes of 1 hour apart. Large systematic variation of the residuals can be removed with these models.

However, small and shorter fluctuations cannot be removed with this model. In our estimation, the scattering of the delay residuals is about 300 ps as a standard deviation. The averaged standard deviations of clock offset and zenith atmospheric delay are 469 ps and 216 ps in our result. As the reference, the result that was estimated from the experiment in Kashima 34m – Mizsawa 10m baseline, November, 1994 are shown. In this result, the post-fit residual was 33 ps as the standard deviation and the standard deviations of clock offset and zenith atmospheric delay were 102 ps and 243 ps.

2) Thermal noise

Thermal noise of the bandwidth-synthesized delay is given by

$$\sigma_\tau = 1/(2\omega_{eff}\,\mathrm{SNR}) \quad , \qquad (5\text{-}1)$$

where σ_τ is a standard deviation of a group delay, ω_{eff} is an effective bandwidth and *SNR* is a signal-to-noise ratio obtained in the bandwidth synthesis. The effective bandwidth is expressed as:

$$\omega_{eff} = \frac{1}{N}\sum_{n=1}^{N}\left(\omega_n - \bar{\omega}\right)^2 \quad and \quad \bar{\omega} = \frac{1}{N}\sum_{n=1}^{N}\omega_n \quad , \qquad (5\text{-}2)$$

where ω_n is a frequency of the n-th channel. If $SNR \geq 6.0$, σ_τ becomes smaller than 2×10^{-10} second for the Syowa experiment where $\omega_{eff} = 133MHz$ in X band(see table 3.4).

Figure 5.4 shows distributions of σ_τ of Hobart - Syowa and Hobart - HartRAO baselines in the present experiment and Hobart – MIZNAO10 baseline in the IRIS-P experiment in July, 1993. MIZNAO10 is the 10m antenna at Mizusawa. The diameter of MIZNAO10 is 10m which is almost the same as that of Syowa. σ_τ of the baselines including SYOWA is larger than that of the other baselines because Syowa's antenna is much smaller than the others. However, it is seen that σ_τ of the present experiment is smaller than that of the IRIS-P. In the IRIS-P experiment the position of MIZNAO10 was estimated with the standard deviation smaller than 2 cm. Therefore, it is not likely that relatively large σ_τ caused the large scatter of the post-fit residuals.

Before the observation, system temperature was not determined in Syowa Station. However, when pointing check was carried out before the start of the VLBI observation, variation of electric power transmitted from the front-end system by the reception of the radio object was almost the same with the inspected value (see table 3.3). Also, since background-noise of the transmission system did not show abnormal variations during the observation, it is considered that the observation system of Syowa VLBI station was stable during the observation.

Figure 5.4 shows a histogram of the standard deviations of the individual observations computed with equation (5-1) for Hobart – Syowa baseline. It has a peak at σ_τ=30 ps and most of the standard deviations are smaller than 50 ps.

3) Errors in the time system transformation

Since the time tags of FITS data are expressed by Julian date in four bytes, the effective ciphers in the time are down only to a microsecond. This time tag is used as a reference epoch in the reduction processing. Namely, the reference epoch of this analysis system is affected by the fluctuation of several microseconds. This fluctuation is preserved during the course of the time system transformation. On the other hand, a rate of a baseline-based delay is a few times of 10^{-8} sec/sec. Accordingly, the error included in the baseline-based delay is estimated to be of the order of 10^{-14} sec.

4) Errors due to inaccurate station and radio source positions

The post-fit residual of 300 ps corresponds to station position error of 9 cm. Similarly, the radio source position error of about one mille-arc-second is necessary to cause the error of 300ps. Since ITRF2000 and ICRF2000, which are currently considered to be most accurate, are used as reference catalogues, it is not likely that these catalogues are affected by such large errors. However, the residual delays shown in figure 5.1 give an impression of smooth and systematic variations specific to individual radio sources. Accordingly, it may be suggested that these catalogues are affected by large errors. The most probable source of the error may be the position of Parkes, since there have been only a few VLBI determinations of its position.

5) Inaccuracy and/or negligence of the adopted geophysical parameters

Some geophysical parameters used in this estimation may not be accurate enough and some are not taken into account. For example, displacements due to the atmospheric loading are set to zero. Typical rate of the vertical displacement is 0.4mm/hPa in a continental region and much smaller in an oceanic region. Since Syowa Station is close to the sea and the air pressure during the experiment was 980hPa, it is not likely that the error due to the negligence of the atmospheric loading contributed largely to the large scattering of the post-fit residuals.

The wobble and UT1 were taken from IERS Bulletin B and interpolated to epochs of the individual scans by polynomial interpolation. Since the Bulletin B values are given every 5 days, short periodic variations such as sub-diurnal variation due to tidal currents cannot be taken into account. However, the interpolation error corresponds to displacement of a few mm (< 30 ps).

Horizontal anisotropy in the mapping function of the zenith atmospheric delay is not taken into account. It has been reported that estimation of the anisotropy as well as the short periodic variation of the zenith delay reduces the post-fit residuals to some extent. Adoption of the anisotropic model may reduce the errors though the amount is not expected to be large enough.

5. Other possibility

The VLBI observation system of Syowa Station is not installed in an optimum environment for high accuracy VLBI experiments. For example, the hydrogen maser frequency standards are placed in bad operational environment without active air conditioning. Although reference signal transmission cables are exposed on the surface of the ground in the severe environment, the means to calibrate electrical path length of the cables is not equipped. Both of these affect the stability of the reference signals.

During the observation, the hydrogen maser frequency standard was stable and its

frequency stability was 10^{-13} - 10^{-15} $\Delta f / f$. As shown in figure 5.4, the individual delay during the observation is seemed to be determined with high accuracy. So, the phase fluctuations of reference signal that give influences to the result of bandwidth synthesis may be small in short-term as less than a few seconds.

However, we were not able to prepare the equipments that determine the long-term change in electric length of reference signal transmission cables. So, the contribution to the post-fit residual is not available. Furthermore, the change of the physical cable length by outside temperature is conceivable as less than a few mm.

5.4 Discussion for the clarification of error factors

The errors in subsection 5.3.3 are divided to three as:

1) Error specific to the experiment in November, 1998.
2) The error in the correlation processing of MFC and/or newly developed analysis software
3) Error specific to Syowa experiment and/or observation system of Syowa Station.

However, these factors cannot be clearly distinguished each other only from the present analysis.

In order to check the first possibility, the other present result has to be compared with those of other Syowa experiments which are presently not available but expected to become available in the near future. The methods to investigate the second and the third possibility are shown in figure 5.5.

In figure 5.5, (a) is a referential geodetic VLBI experiment with accurate station and radio source positions and reliable observation systems. (A) is a correlator of established accuracy. GSI's correlator is an example of such correlator. Geodetic result obtained with a combination of (a) and (A) becomes the reference solution to the Syowa experiment and newly developed analysis system for MFC.

The comparison of the two combinations, (a)-(A) and (a)-(B), discriminates the influence of the difference between two analysis systems, (A) and (B). Reliability of B can be confirmed by this work. If the two combinations, (b)-(A) and (b)-(B) yield the same results, the reliability of the geodetic result of the present Syowa experiment is considered to be confirmed.

5.5 Comparison with other estimations of Syowa's position and velocity

There are several observational determinations and model predictions of the position and velocity of Syowa Station. We compare our results with them in this section. The observational determinations to be compared are those obtained from the VLBI observation during JARE30 in 1990 (Kurihara et al., 1995) and JARE40 in 1999. The JARE40 results are derived from the CORE-OHIG VLBI observations and given in ITRF2000_VLBI.SSC. The satellite results by GPS and DORIS are also compared. As for the model prediction, the NNR-NUVEL1A plate motion model is compared.

5.5.1. The first VLBI experiment at Syowa Station in 1990 by JARE30

The coordinates of the Syowa VLBI reference point were determined by JARE30 (Kurihara et al., 1995). This report presented the coordinates of the Syowa VLBI reference as:

$$X= 1766194.099\text{m} \quad \sigma_X=0.061\text{m}$$
$$Y= 1460410.899\text{m} \quad \sigma_Y=0.010\text{m}$$
$$Z=-5932273.311\text{m} \quad \sigma_Z=0.096\text{m}$$

in ITRF92 at the epoch 1992.0.

5.5.2. ITRF2000 and the VLBI experiment in November, 1999

The coordinates at January 1, 1997, and velocities of the Syowa VLBI reference point are given in ITRF2000_VLBI.SSC. These coordinates were determined from three observations called CORE-OHIG carried out on November 8, 10 and 11 in 1999 during JARE40 and on February 10 in 2000 in immediately after that JARE41 starts the wintering. The observation network consists of Fortareza in Brazil, Kokee Park in Hawaii, HartRAO in South Africa, O'Higgins in Antarctic Peninsula, Hobart in Australia and Syowa in Antarctica. All of the stations except for Kokee Park are located in the southern hemisphere. The data were analyzed by Bonn University. Since the observation period spans only three months, which are not long enough to determine velocities, the velocities common to those of IGS and DORIS observation points are given in the catalogue.

The coordinates of the Syowa VLBI point at the observations in November, 1999 (epoch=1999.9), are computed from the coordinates and velocities in ITRF2000 as:

$$X= 1766194.151\text{m} \quad \sigma_X=0.013\text{m}$$
$$Y= 1460410.945\text{m} \quad \sigma_Y=0.013\text{m}$$

$$Z=-5932273.377\text{m} \quad \sigma_Z=0.027\text{m}.$$

The velocity of Syowa Station in ITRF2000 is given as:

$$V_X= 3.8\text{mm/y} \quad \sigma_{VX}=0.8\text{mm/y}$$
$$V_Y=-1.5\text{mm/y} \quad \sigma_{VY}=0.8\text{mm/y}$$
$$V_Z=-1.5\text{mm/y} \quad \sigma_{VZ}=1.8\text{mm/y},$$

where V_X, V_Y and V_Z are the x-, y- and z-components of velocity in the geocentric Cartesian coordinate system.

5.5.3. Velocity of IGS point in Syowa Station

The Syowa IGS station is located on a dew rock and its distance from the MPA is only several hundred meters. It is, therefore, conjectured that MPA and IGS point are built on the same base-rock and the tectonic motion is considered to be almost the same with each other.

GSI/NIPR estimated velocity of IGS Syowa station by using the GPS data obtained during the period from July, 1996, to June, 1997 (Yamada et al., 1998). Their result is given by:

$$V_X= 6.9\text{mm/y} \quad \sigma_{VX}=0.4\text{mm/y}$$
$$V_Y=-0.6\text{mm/y} \quad \sigma_{VY}=0.4\text{mm/y}$$
$$V_Z=-5.9\text{mm/y} \quad \sigma_{VZ}=0.9\text{mm/y}$$

in ITRF2000 system.

JPL is one of the IGS analysis centers. Syowa's IGS point by JPL is given in ITRF2000 and the time series of site's position is disclosed (figure 5.6). Velocity vector in ITRF2000 estimated by JPL is given by

$$V_X= 4.7\text{mm/y} \quad \sigma_{VX}=0.6\text{mm/y}$$
$$V_Y=-3.8\text{mm/y} \quad \sigma_{VY}=0.5\text{mm/y}$$
$$V_Z=-4.6\text{mm/y} \quad \sigma_{VZ}= 1.2\text{mm/y}.$$

Direction of this velocity vector is different largely from the result of GSI/NIPR. The GPS receiver was renewed in 2000. The renewal of the GPS receiver might have affected the estimation of the velocity vector. The solution obtained from the accumulated data by the new receiver is desired.

5.5.4. Velocity predicted by a global plate motion model

The NNR-NUVEL1A global plate motion model predicts the velocity of the Syowa VLBI point to be:

$$V_X=4.3\text{mm/y},\ V_Y=2.0\text{mm/y},\ V_Z=1.8\text{mm/y}.$$

5.5.5. Velocity of the Syowa DORIS station

The Syowa DORIS station is established near the earth science hut and its distance from the MPA is several hundred meters. The movement of DORIS station was estimated by JPL and given in ITRF97, which was released to ITRF first among the space geodetic observation points in Syowa Station.

The velocity vector of Syowa DORIS Station is expressed as:

$$V_X= 13.5\text{mm/y}\quad \sigma_{VX}=4.3\text{mm/y}$$
$$V_Y=-6.2\text{mm/y}\quad \sigma_{VY}=4.2\text{mm/y}$$
$$V_Z=-3.8\text{mm/y}\quad \sigma_{VZ}= 4.8\text{mm/y}$$

in ITRF97.

LEGOS/CLS (Laboratoire dEtudes en Geophysique et Oceanographie Spatiales / Collecte, Localisation, Satellites), which is one of the DORIS analysis center, discloses the monthly solutions of DORIS observation points in the world. Figure 5.7 shows the monthly solution of the Syowa DORIS station. The velocity vector is given by

$$V_X=10.5\text{mm/y},\ V_Y=-7.1\text{mm/y},\ V_Z=0.7\text{m/y}$$

in ITRF97.

5.5.6. Position and Velocity of the Syowa space geodetic observation points in ITRF2000

The above positions and velocities described in subsections 5.3.1- 5.3.5 are expressed in different terrestrial reference frames (TRF's). Mutual comparison requires that positions and velocities be expressed in a common reference frame. ITRF2000 is adapted as a common TRF for the intercomparison of the above positions and velocities because our result is estimated in ITRF2000. Details of the coordinate transformations are described in Appendix B and the only results are summarized here.

The VLBI result at 1990.1 described in subsection 5.3.1 are transformed to

X=1766194.082m, Y=1460410.887, Z=-5932273.290m

in ITRF2000.

The velocities of the IGS and DORIS points are shown in table 5-3 and the velocities of VLBI point obtained from three VLBI experiments are shown in tables 5-4a and 5-4b.

Table 5.4a. Velocity of the Syowa VLBI point in geocentric Cartesian system.

Component	V_X	V_Y	V_Z	σ VX	σ VY	σ VZ
Unit	(mm/y)	(mm/y)	(mm/y)	(mm/y)	(mm/y)	(mm/y)
Velocity	6.9	5.8	-9.0	6.3	1.5	10.1

Table 5.4b. Velocity of the Syowa VLBI point in the local topocentric system

Component	V_N	V_E	V_U	σ VN	σ VE	σ VU
Unit	(mm/y)	(mm/y)	(mm/y)	(mm/y)	(mm/y)	(mm/y)
Velocity	5.3	0.1	11.7	2.2	1.7	10.0

5.5.7. Intercomparison of the determinations

The above five positions and velocities are compared in tables 5.5 and 5.6. They are also shown in figures 5.8 and 5.9. The positions are given as differences from our result. The coordinates, velocities and their error bars given in table 5.5 and figure 5.8 are expressed in the geocentric Cartesian system and those given in table 5.6 and figure 5.9 are expressed in the local topocentric system.

Error bars of the coordinates of VLBI position shown in figure 5.8 are estimated with the VLBI position. Other error bars in figure 5.9 are calculated from errors associated with velocity vectors of the Syowa IGS and DORIS stations.

On the other hand, error bars other than those of VLBI at 1998.9 shown in figure 5.9 are not exact, since full covariance matrices of the estimated coordinates are not available. These error bars are computed on the assumption that principal axes of the error ellipsoid coincide with the x, y and z directions. This assumption may be justified by the facts that: 1) in estimation of ground position using space geodesy, the longest axis of error ellipsoid almost coincides with the vertical axis to the ground, 2) in high latitude area as Syowa Station, the vertical axis to the ground is close to the z-axis of the geocentric Cartesian system.

It seems that the VLBI point is moving almost linearly with time although the errors

are not small enough to derive a definitive conclusion. The point obtained from VLBI is moving almost northward in the horizontal plane. The direction of the vertical motion is uplifting.

Speeds of the horizontal movements are almost the same for VLBI, GPS and NNR-NUVEL1A. Speed of DORIS point is about twice faster than the others. The moving directions of VLBI and NNR- NUVEL1A are close with each other, while those of GPS, DORIS are not. Moving direction of ITRF2000 is similar to DORIS's. Speed of ITRF2000 is the smallest in these movements. The vertical velocities of GPS (NIPR/GSI, JPL), DORIS (JPL) and ITRF2000 seem to be supportive to the uplifting motion obtained by VLBI although these magnitudes are smaller than VLBI's.

Table 5.5. Comparison of the various determinations and predictions of the Syowa position expressed as differences from the VLBI estimation at 1998.9 in the geocentric Cartesian coordinates. The positions of GPS and DORIS are computed by using the velocities, since there is no accurate tie among the VLBI, IGS and DORIS points. NUVEL1A and ITRF2000 are also computed from the velocities. 1990 and 1999 symbolically denote the epochs of the VLBI observations.

Source	epoch	dX (cm)	dY (cm)	dZ (cm)	σ X (cm)	σ Y (cm)	σ Z (cm)
VLBI	1990.1	-6.1	-4.5	6.3	6.1	1.0	9.6
VLBI	1998.9	0.0	0.0	0.0	2.9	2.5	6.2
VLBI	1999.9	0.7	1.3	-2.4	1.3	1.3	2.7
GPS (NIPR/GSI)	1990.1	-6.2	-0.2	4.0	0.1	0.1	0.3
GPS (NIPR/GSI)	1999.9	0.7	0.0	-0.4	0.0	0.0	0.1
GPS (JPL)	1990.1	-4.1	3.3	4.1	0.2	0.2	0.4
GPS (JPL)	1999.9	0.5	-0.4	-0.5	0.1	0.1	0.1
DORIS (LEGOS/CLS)	1990.1	-9.4	5.9	-1.8	0.2	0.2	0.2
DORIS (LEGOS/CLS)	1999.9	1.0	-0.6	0.2	0.1	0.1	0.1
DORIS (JPL)	1990.1	-12.0	5.1	2.1	1.3	1.3	1.4
DORIS (JPL)	1999.9	1.3	-0.5	-0.2	0.4	0.4	0.5
NUVEL1A	1990.1	-3.8	-1.8	-1.6	-	-	-
NUVEL1A	1990.9	0.4	0.2	0.2	-	-	-
ITRF2000	1990.1	-3.3	1.3	1.3	0.2	0.2	0.5
ITRF2000	1999.9	0.4	-0.2	-0.2	0.1	0.1	0.2

Table 5.6 The same as table 5.4.but in the local topocentric system. Errors are not exactly other than those of VLBI at 1998.9, since full covariance matrix are not available. Since plates are assumed to slip on the surface of the earth in NNR-NUVEL1A, the vertical component of displacement is zero.

Source	epoch	d_{NS} (cm)	d_{EW} (cm)	d_{UD} (cm)	σ_{NS} (cm)	σ_{EW} (cm)	σ_{UD} (cm)
VLBI	1990.1	-4.8	0.4	-8.6	1.9	1.3	9.6
VLBI	1998.9	0.0	0.0	0.0	2.1	1.8	6.7
VLBI	1999.9	0.4	0.6	2.7	1.3	1.3	2.7
GPS (NIPR/GSI)	1990.1	-3.1	3.8	-5.4	0.1	0.1	0.3
GPS (NIPR/GSI)	1999.9	0.4	-0.4	0.6	0.0	0.0	0.1
GPS (JPL)	1990.1	0.5	5.2	-4.2	0.2	0.2	0.4
GPS (JPL)	1999.9	-0.1	-0.6	0.5	0.1	0.1	0.1
DORIS (LEGOS/CLS)	1990.1	-3.9	10.5	0.4	0.2	0.2	0.2
DORIS (LEGOS/CLS)	1999.9	0.5	-1.1	-0.1	0.1	0.1	0.1
DORIS (JPL)	1990.1	-4.8	11.5	-4.1	1.3	1.3	1.4
DORIS (JPL)	1999.9	0.6	-1.3	0.4	0.4	0.4	0.5
NUVEL1A	1990.1	-4.3	1.0	0.0	-	-	-
NUVEL1A	1990.9	0.5	-0.1	0.0	-	-	-
ITRF2000	1990.1	-1.1	3.1	-1.8	0.2	0.2	0.5
ITRF2000	1999.9	0.1	-0.4	0.3	0.1	0.1	0.2

5.6 Geodetic interpretations

The relative motion among the geological units that compose the Antarctic Plate is the most interesting subject of Antarctic geoscience. Kubo et al. (1998) derived anomalous motion of 6 IGS points in Antarctica including Syowa (figure 5.10). The deviations of velocities from the rigid plate motion model vary from 1mm/y to 5mm/y. Since standard deviations of anomalous velocities of 4 out of the 6 points are sufficiently smaller than the velocities, these anomalous velocities are considered to be statistically significant. However, this does not mean that intra-plate motion has been detected. The distributions of the IGS points are very sparse and velocity vectors do not show systematic trend. In fact, velocity vectors of the two IGS points in Antarctic Peninsula are almost opposite each other. Therefore, anomalous velocities derived by Yamada et al. (1998) are considered to be strongly affected by local crustal fluctuations.

The estimated horizontal movements of Syowa Station can evidently be classified to two groups. One is composed of VLBI and NUVEL1A, which are moving almost northward. The other is composed of DORIS, IGS (NIPR/GSI) and ITRF2000, which move along the northwest direction.

Since Syowa Station is located on the continental shield composed of the old base-rock, the rigid plate model is considered to be a good approximation to the motion of the geodetic observation points in Syowa Station. Close agreement of the horizontal movements between the VLBI observations and the NNR-NUVEL1A prediction may support the rigid plate motion model. Namely, it means that local movement in the horizontal plane is almost nonexistent. This contradicts the results of the other space-geodetic techniques.

Odamaki et al. (1991) estimated a sea level change of 9.5mm/y at Syowa Station using annual means of mean sea level obtained from the tide gauge data from 1981 to 1987. The VLBI estimate of the upheaval from 1990 to 1999 is 11.3 cm. This speed corresponds to the upheaval of 11.7mm/y and is not contradictory with the sea level change. Furthermore, Kaminuma's (1985) estimate of the upheaval as the PGR, which is obtained from the upheaval of the seashore lines and radiated carbon age of the shellfish fossils in the Ongul Islands periphery, is 4mm/y. Although VLBI estimate is also not contradictory to the upheaval of the seashore lines in direction, magnitude is larger in compared to Kaminuma's estimate. The vertical velocity derived from ITRF2000 also shows the upheaval of Syowa Station though it is 1.8mm/y. Also most of the vertical movements at the other space-geodetic observation points support the uplifting trend of the crust. Therefore, it is likely that our estimate of the upheaval

velocity reflects PGR in some extent. However, since our estimate has an error of 10.0mm/y, further observations are necessary for deriving a conclusive value.

Also, it is interesting to temporally trace the differences of the upheaving rates for clarifying the relation among these rates, microseismic activity in the Ongul Islands periphery and detailed crustal deformation associated with PGR.

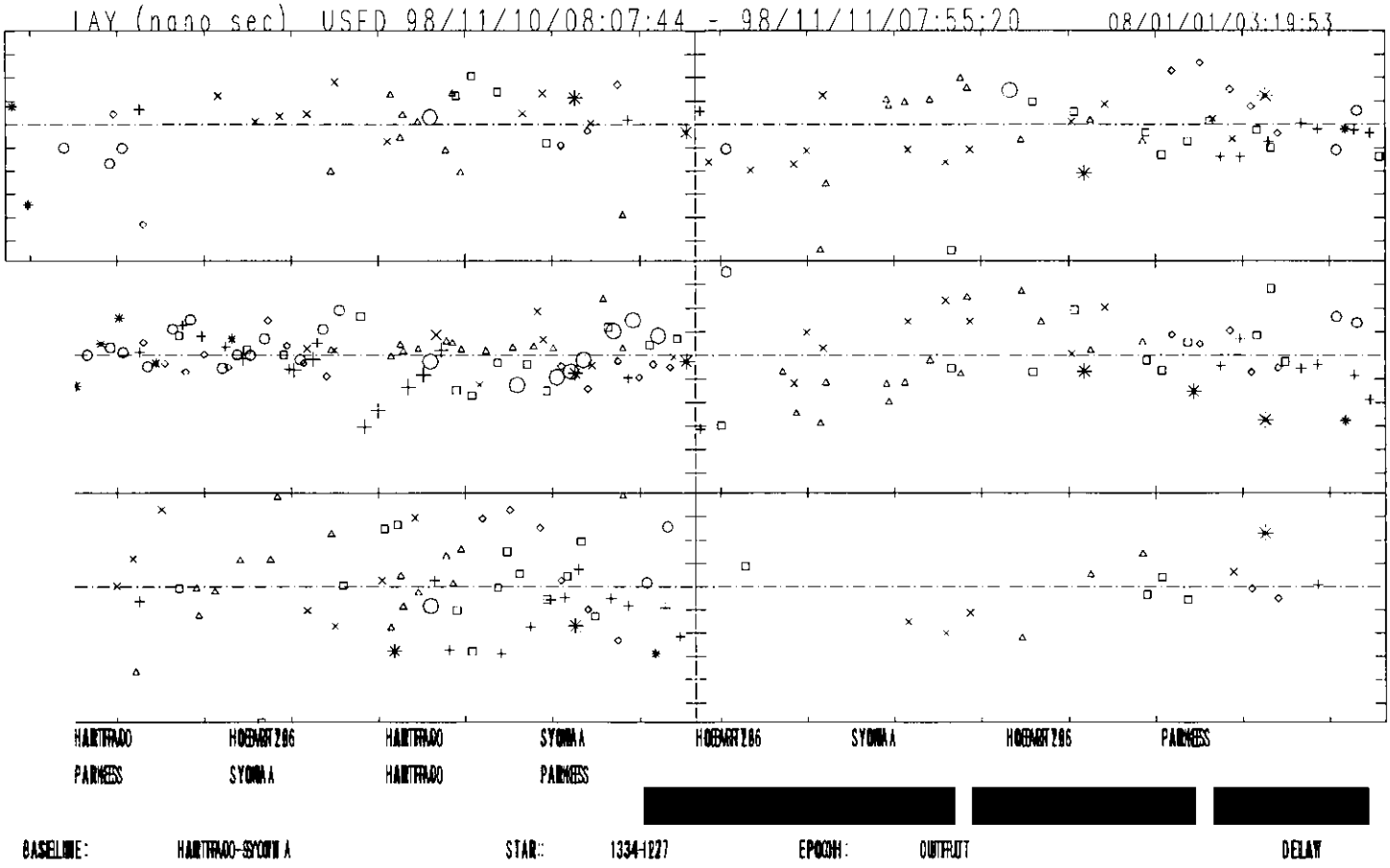

Figure 5.1 Post-fit residual delays of the individual baselines. Ordinate is residual delay. One tick interval is 0.1ns. Abscissa is time with 3 hours as one tick interval. Baselines are, from top left to bottom right columnwise, HartRAO-Hobart, Syowa-Hobart, Hobart-Syowa, Hobart-Parkes, Parkes-Syowa and HartRAO-Parkes.

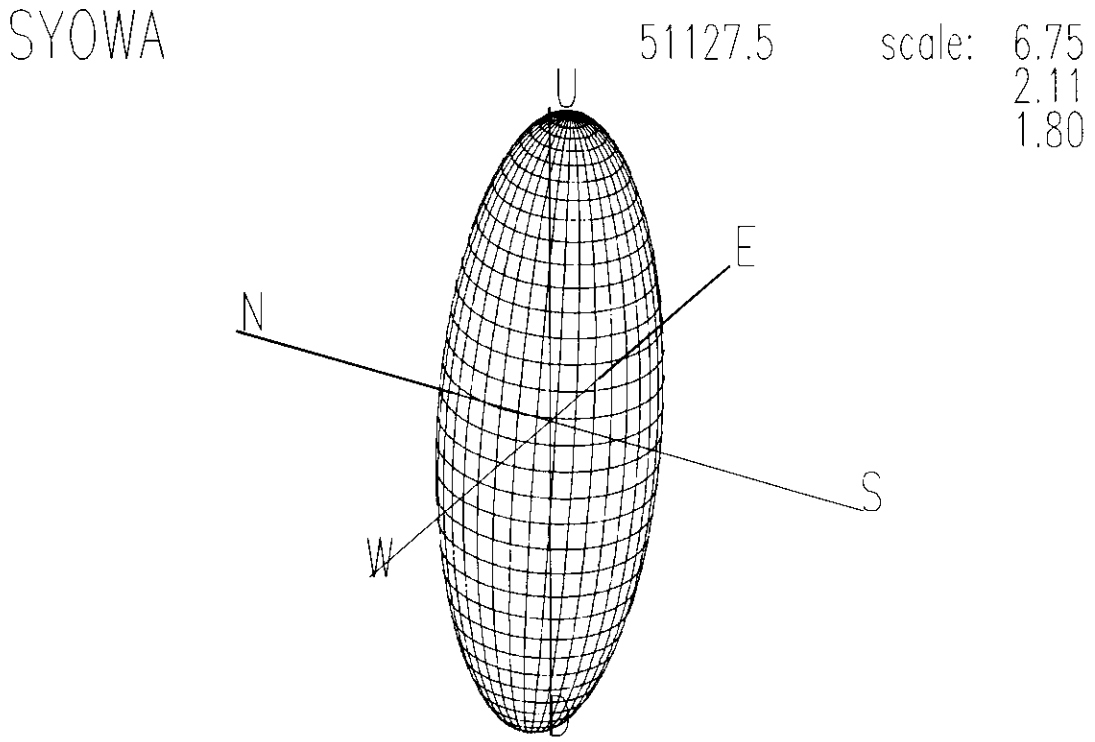

Figure 5.2 Error ellipsoid of the estimated position of Syowa. scale in the top-right of the figure shows length of principal axes in cm. Note that the major axis almost coincides with the vertical axis..

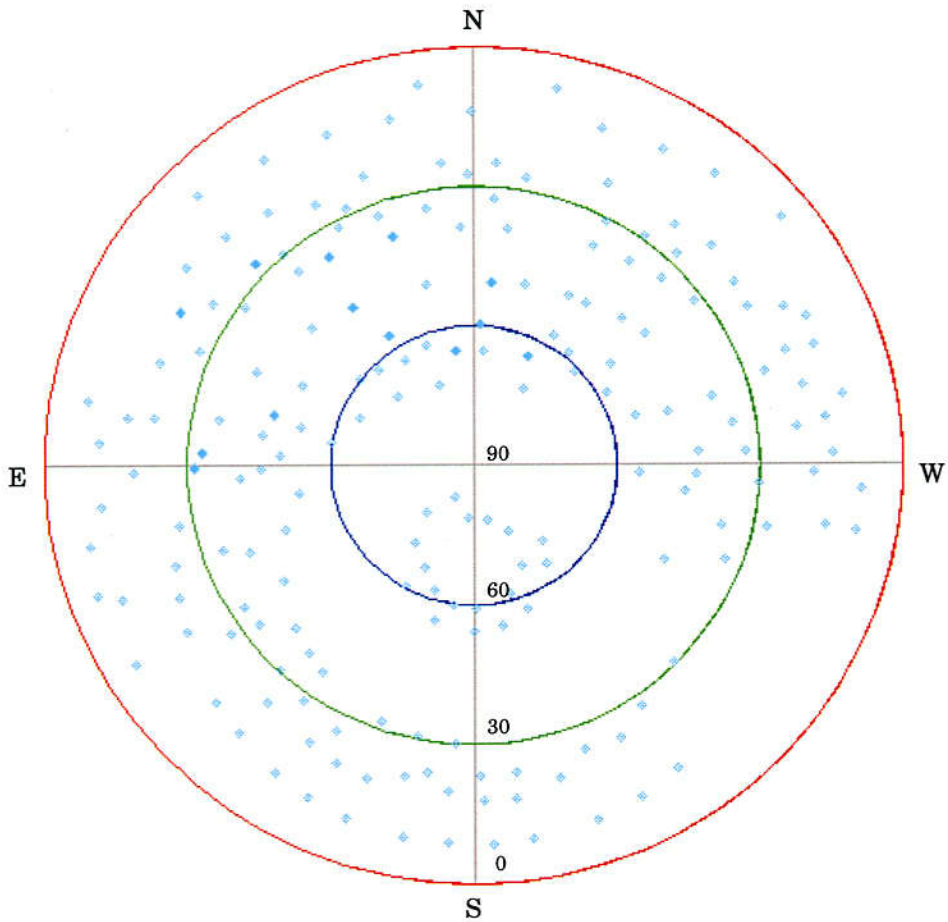

Figure 5.3. Distribution of observed directions in the celestial semisphere at Syowa Station. These VLBI experiment is SYW984 in November, 1998.

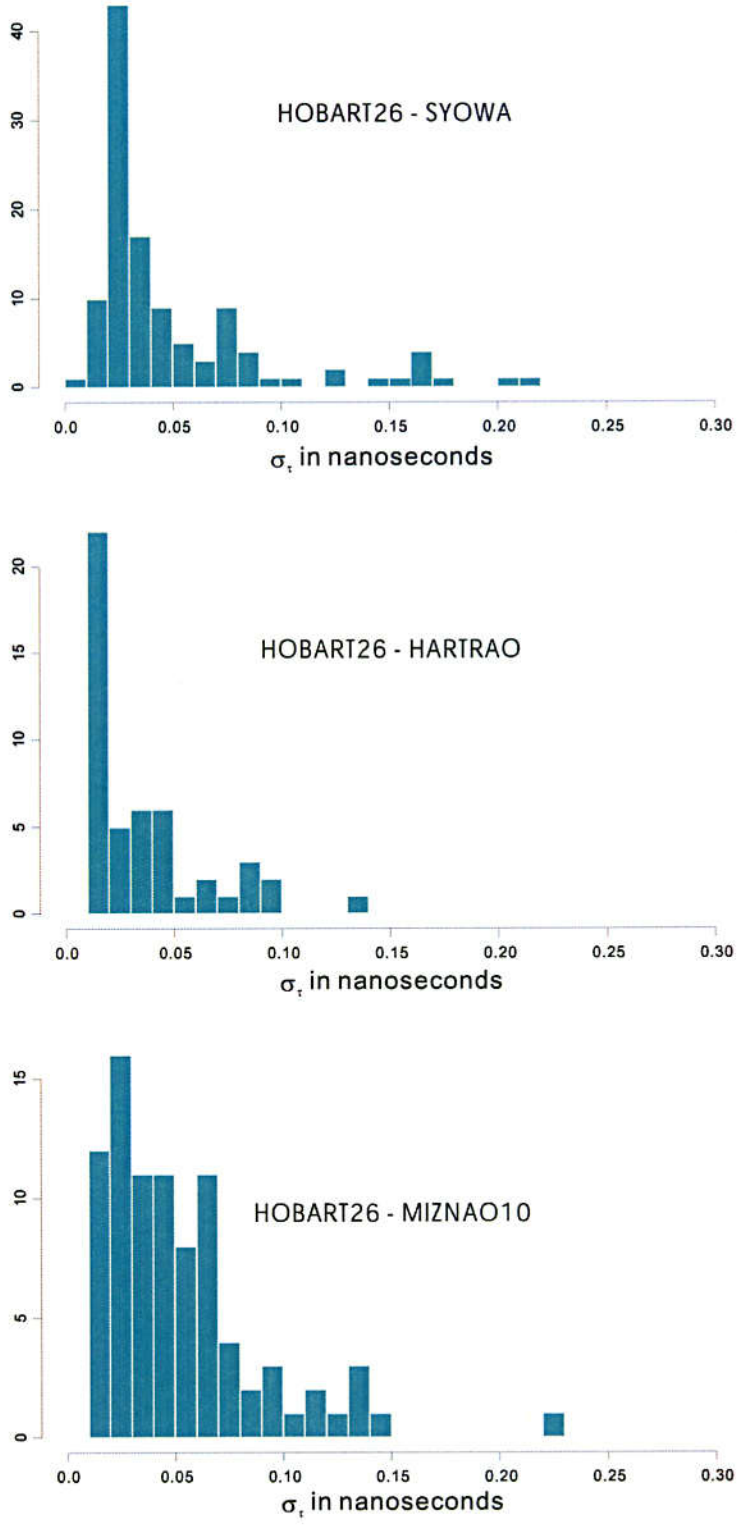

Figure 5.4 Histograms standard deviations of individual delays. The standard deviations are given by equation 5-1. Baselines are, from top to bottom, Hobart-Syowa and Hobart-HartRAO in this analysis, and Hobart-Mizusawa 10m in IRIS-P in 1993.

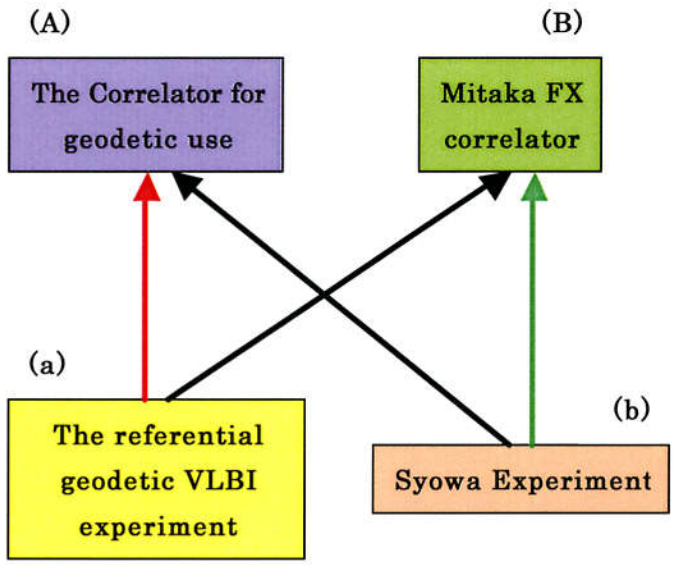

Figure 5.5 The cross check diagram between the correlators and geodetic VLBI experiments. The geodetic result that is produced by the combination of (a) and (A) becomes a reference solution to the combination of (b) and (B).

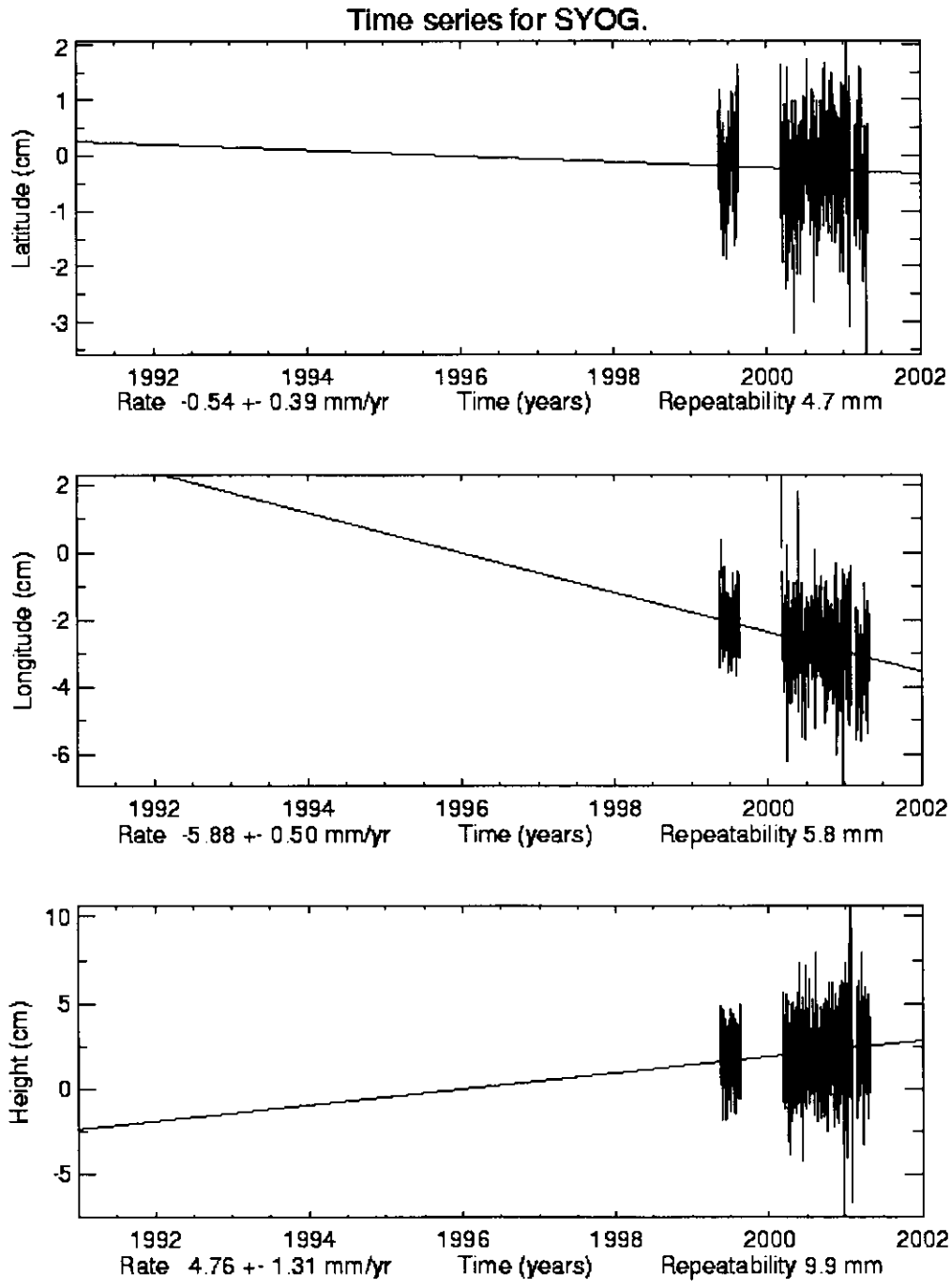

Figure 5.6. Time series of daily solutions at Syowa IGS point. Fiducial Laboratories for an International Natural Science Network, JPL are discloses in its website.

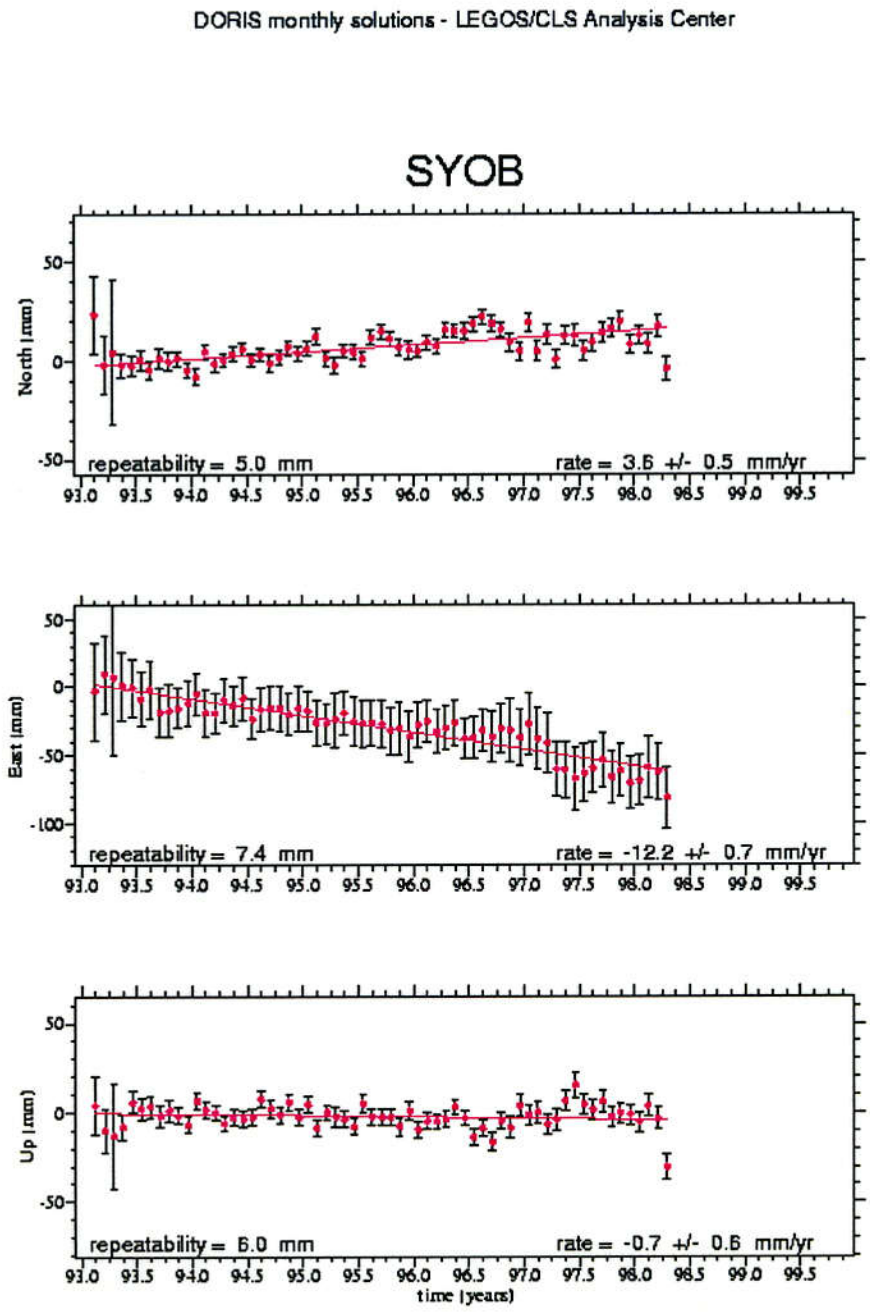

Figure 5.7. Time series monthly solutions at Syowa DORIS point. This is disclosed in International DORIS Service.

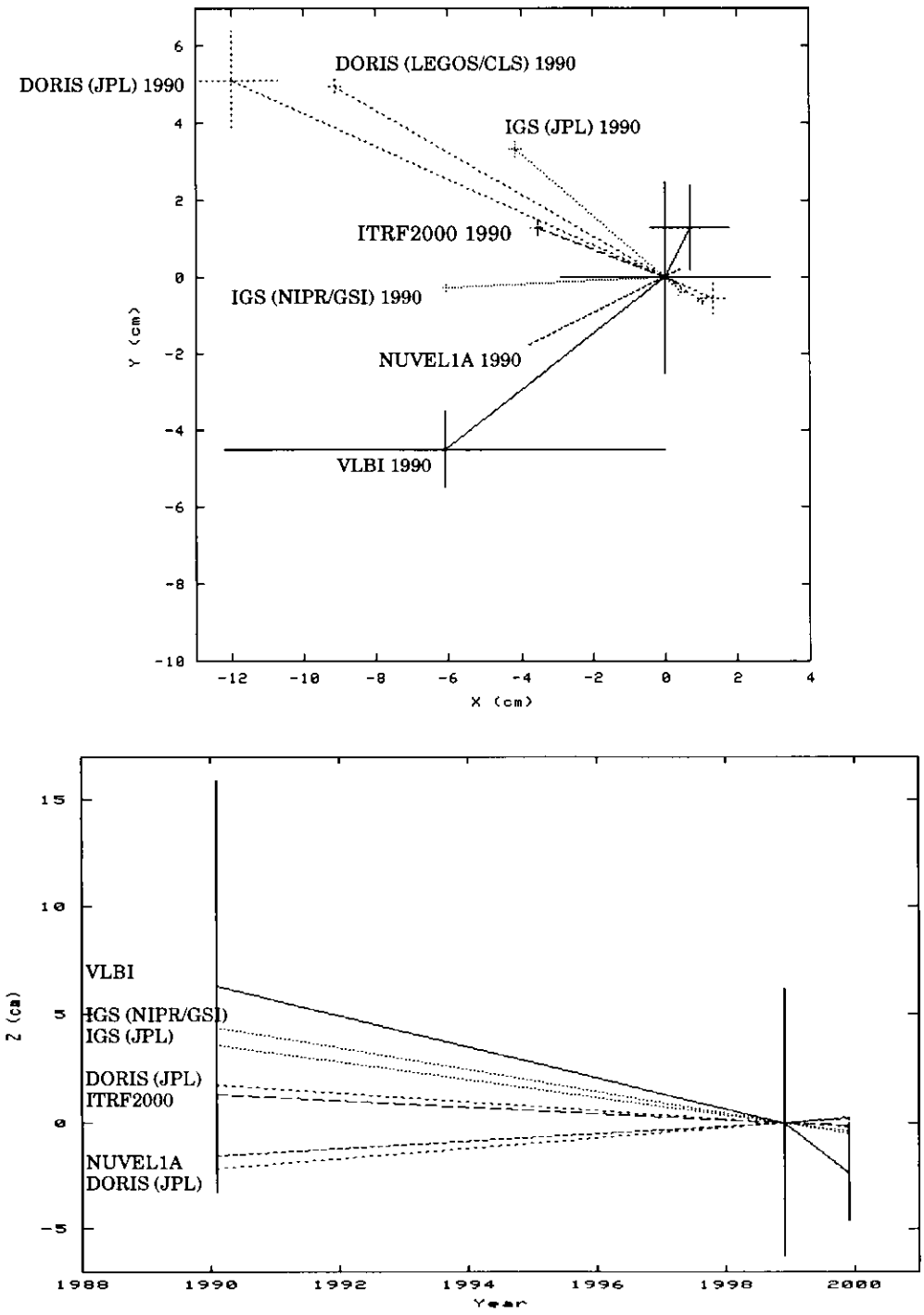

Figure 5.8 Comparison of various estimates and prediction of Syowa's position. The upper figure shows the x and y components, while the lower show the z coordinate versus time. Positions in 1990 and 1999 are expressed as differences from our result in 1998. It is to be noticed that the general trend of the motion of the VLBI point agrees well with the prediction by the plate motion model.

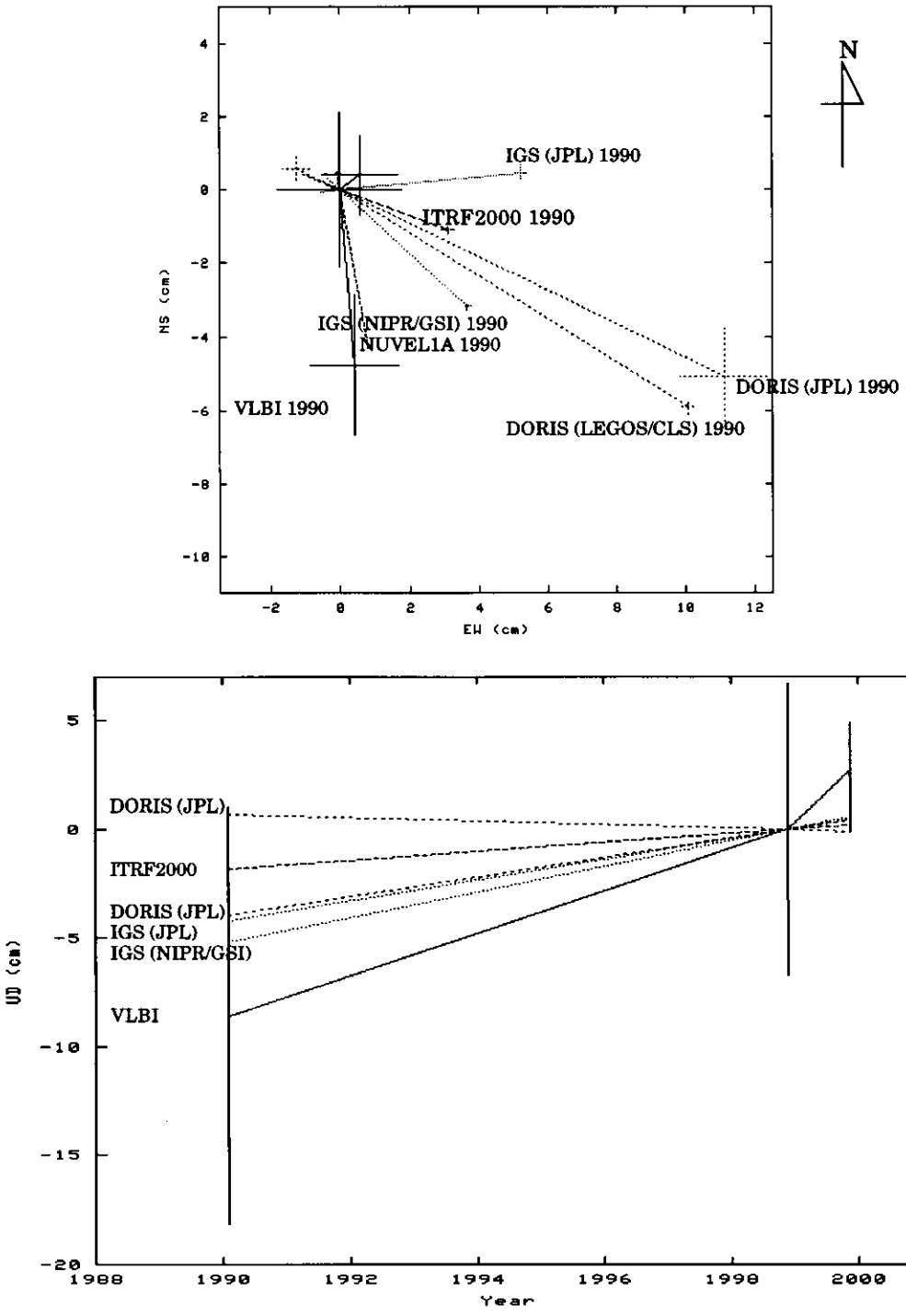

Figure 5.9 The same as those in figure 5.4 but displacements are shown in the local topocentric system. The upper figure shows the horizontal movements and the lower shows the time variation of the vertical components which may reflect PGR.

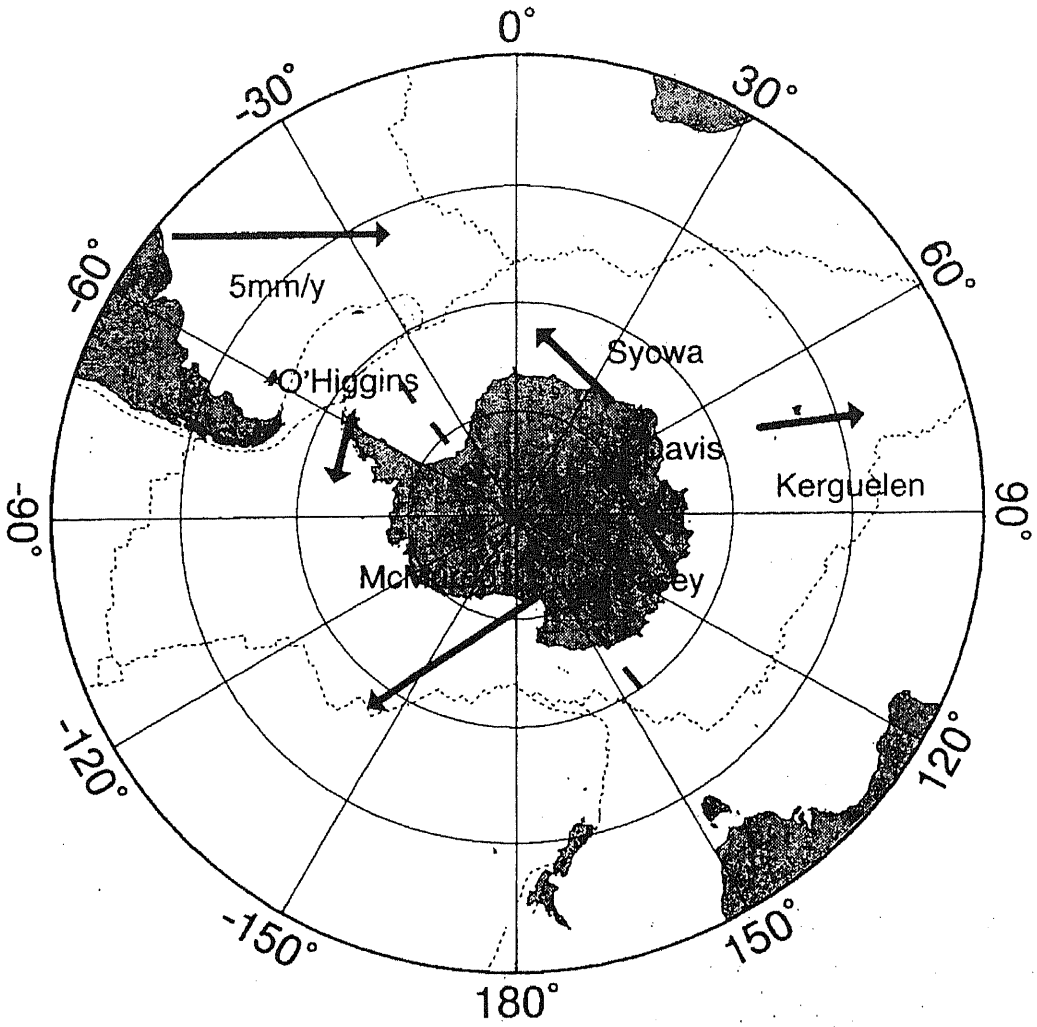

Figure 5.10. Residual motions obtained by subtracting fitted rigid plate motion in the Antarctic plate (Reproduced from Yamada et al., 1998). The broken line shows the Transantarctic mountains. (Referred to Kubo et al., 1998).

6. Summary and conclusion

The regular VLBI experiment was initiated at Syowa Station in JARE39 as one of the important research subjects of sciences of Antarctica. This experiment is resumed for the first time after 9 years interruption and continuous observations are under way. JARE39 constructed the Syowa VLBI observation system in the summer operation and carried out four experiments in the wintering. Although various problems occurred during the JARE39 operation, smooth operation is carried out in JARE40 and succeeding expeditions by utilizing the experiences in JARE39.

The MFC was used in the correlation processing, since the Antarctic VLBI network uses two types of recorders, K4 and S2, for recording VLBI raw data. The new geodetic analysis system was developed for reducing the data correlated with the MFC, since no such system was available.

The position of the Syowa VLBI geodetic reference point was determined with this new geodetic analysis software. The errors are about 2cm for the horizontal components and about 7cm for the vertical component. The scattering of the post-fit residual delays is nominally 300 ps which is much larger than a typical value of recent geodetic VLBI observation. The reason of this large error is discussed but it is yet unclear. To search the causes of this large error, discrimination of the observation's errors and the analysis' errors is needed. Comparison of two results, which are estimated from the VLBI geodetic analyses by the newly developed analysis system and regularly used geodetic analysis system, enables to clarify the errors that are specific to the MFC and new analysis software. These works are necessary to confirm the reliability of our analysis system.

The movement of Syowa VLBI reference point was estimated from three VLBI results of 1990, 1998 (this study) and 1999 experiments. The horizontal movement agrees closely with the predicted movement by NNR-NUVEL1A global plate motion model. The vertical movement is not contradictory to the trend obtained from the tide gauge and geological survey. However, the large standard deviations of the estimated positions prevent to derive definitive conclusions on the plate motion and the PGR. A reliable detection of these is expected with the improved estimation of the Syowa VLBI point by analyzing data taken in JARE40 and subsequent expeditions.

The main part of the geodetic analysis system for the MFC is considered to be usable as one of the core parts of a VERA analysis system and a large contribution is expected in the VERA project.

Appendix A Initial coordinates of stations and radio sources

Table A-1 Station coordinates at November 10, 1998 based on ITRF2000

Station	x(m)	y(m)	z(m)
HARTRAO	5085442.7777	2668263.5287	-2768696.9829
HOBART26	-3950236.8149	2522347.5776	-4311562.4611
SYOWA	1766194.1464	1460410.9481	-5932273.3739
PARKES	-4554232.0965	2816758.9637	-3454035.7724

Table A-2 Radio source coordinates taken from ICRF2000

Name	Right ascension			Declination		
	hour	min	sec	deg	min	sec
1057-797	10	58	43.30979	-80	3	54.15949
1921-293	19	24	51.05596	-29	14	30.12115
1741-038	17	43	58.85614	-3	50	4.61668
1958-179	20	0	57.09045	-17	48	57.67251
0208-512	2	10	46.20041	-51	1	1.89200
1034-293	10	37	16.07973	-29	34	2.81322
0537-441	5	38	50.36155	-44	5	8.93908
1954-388	19	57	59.81927	-38	45	6.35626
0637-752	6	35	46.50793	-75	16	16.81533
1144-379	11	47	1.37070	-38	12	11.02353
2145+067	21	48	5.45868	6	57	38.60422
1334-127	13	37	39.78278	-12	57	24.69323
0048-097	0	50	41.31739	-9	29	5.21021
0003-066	0	6	13.89289	-6	23	35.33530
1424-418	14	27	56.29756	-42	6	19.43762
0727-115	7	30	19.11247	-11	41	12.60048
0528+134	5	30	56.41674	13	31	55.14955
0104-408	1	6	45.10797	-40	34	19.96036
1610-771	16	17	49.27640	-77	17	18.46743

Appendix B The unification of the reference frames

The transformation formula of coordinates from a terrestrial reference frame a to a terrestrial reference frame b is expressed as:

$$\mathbf{X}_b(t) = \mathbf{A}(t)\mathbf{X}_a(t),$$
$$\dot{\mathbf{X}}_b = \dot{\mathbf{A}}\mathbf{X}_a(t) + \mathbf{A}(t)\dot{\mathbf{X}}_a,$$

$$\mathbf{A}(t) = \begin{pmatrix} 1+D(t) & -R_3(t) & R_2(t) & T_1(t) \\ R_3(t) & 1+D(t) & -R_1(t) & T_2(t) \\ -R_2(t) & R_1(t) & 1+D & T_3(t) \\ 0 & 0 & 0 & 1 \end{pmatrix} \qquad \text{(B-1)}$$

$$\mathbf{X}_a(t) = (X_a(t) \quad Y_a(t) \quad Z_a(t) \quad 1)^T,$$
$$\mathbf{X}_b(t) = (X_b(t) \quad Y_b(t) \quad Z_b(t) \quad 1)^T,$$

where X_a, Y_a, Z_a are coordinates in a-TRF, X_b, Y_b, Z_b are coordinates in b-TRF, T_1, T_2, T_3 are the components of a translation vector, D is a scale factor and R_1, R_2, R_3 are the components of an infinitesimal rotation matrix. Let P be a set of the seven transformation parameters T_1, T_2, T_3, D, R_1, R_2, R_3.

The transformation formula from TRF-b to TRF-b is a inverse transformation of equation (B-1) and expressed as:

$$\begin{aligned} \mathbf{X}_a(t) &= \mathbf{A}^{-1}(t)\mathbf{X}_b(t) \\ \dot{\mathbf{X}}_a &= \dot{\mathbf{A}}^{-1}\mathbf{X}_b(t) + \mathbf{A}^{-1}(t)\dot{\mathbf{X}}_b \end{aligned} \qquad \text{(B-2)}$$

Table B-1 shows the position of the VLBI reference point at 1990.1 given in Kurihara(1995) and table B-2 shows the velocities of the Syowa IGS and DORIS points, which refer to the TRFs other than ITRF2000. IGS (NIPR/GSI) is referred Yamada et al. (1998), DORIS (LEGOS/CLS) is taken from the homepage of LEGOS/CLS DORIS analysis center and DORIS (JPL) is given by ITRF97_DORIS.SSC (IERS).

Table B-1. Original Syowa VLBI position estimated from the Syowa VLBI experiments. X, Y and Z are components of the position vector in geocentric Cartesian coordinate system

Source	X(m)	Y(m)	Z(m)	obs. epoch	frame
1990, Jan.	1766194.099	1460410.899	-5932273.311	1990.1	ITRF92

Table B-2. Velocities of the space geodetic observation points in Syowa Station. V_X, V_Y and V_Z are components of the velocity vectors in cm/y.

Source		V_X	V_Y	V_Z	Frame
IGS	NIPR/GSI	0.69	-0.06	-0.59	ITRF94
DORIS	LEGOS/CLS	1.05	-0.71	0.07	ITRF97
	JPL	1.35	-0.62	-0.38	ITRF97

In order to estimate velocity of the VLBI determination of the Syowa VLBI reference point and compare it with those shown in table B2, these position and velocities are made refer to ITRF2000.

Table B-3 shows the seven parameters P which transform ITRF2000 to the individual frames at the epoch indicated in the table.

Table B-3. Transformation parameters from ITRF2000 to other TRFs. These parameters are taken from "ftp://lareg.ensg.ign.fr/pub/itrf/ITRF.TP"

		$T_1/\dot{T}_1$	$T_2/\dot{T}_2$	$T_3/\dot{T}_3$	$D/\dot{D}$	$R_1/\dot{R}_1$	$R_2/\dot{R}_2$	$R_3/\dot{R}_3$	Epoch
Units		cm	cm	cm	ppb	.001"	.001"	.001"	year
		cm/y	cm/y	cm/y	ppb/y	.001"/y	.001"/y	.001"/y	
ITRF92	P_{92}	1.47	1.35	-1.39	0.75	0.00	0.00	-0.18	1988.0
	$\dot{P}_{92}$	0.00	-0.06	-0.14	0.00	0.00	0.00	0.02	
ITRF94	P_{94}	0.67	0.61	-1.85	1.55	0.00	0.00	0.00	1997.0
	$\dot{P}_{94}$	0.00	-0.06	-0.14	0.00	0.00	0.00	0.02	
ITRF97	P_{97}	0.67	0.61	-1.85	1.55	0.00	0.00	0.00	1997.0
	$\dot{P}_{97}$	0.00	-0.06	-0.14	0.00	0.00	0.00	0.02	

The transformation parameter set P at an arbitrary epoch t is computed with

$$P(t) = P(t_0) + (t - t_0)\dot{P} \quad , \qquad (B\text{-}3)$$

where t_0 is any of the reference epochs in table B-3.

The transformation parameter set P_{92} which transforms the reference frame of the Syowa VLBI reference point shown in table B-1 from ITRF92 to ITRF2000 at 1990.1is given by equation (B-3) as:

$$P_{92}(1990.1)=[1.47,\ 1.22,\ -1.68,\ 0.75,\ 0.0,\ 0.0,\ -0.14],$$

where units of P_{92} are to the same as those in table B-3. By substituting this parameter set to equation (B-2), the coordinates of VLBI reference point in ITRF2000 at 1990.1 are given as:

X=1766194.082m, Y=1460410.887m, Z=-5932273.290m.

In order to convert the reference frames of the satellite determinations of the velocities in table B-2 to ITRF2000 by using equation (B-2), the positions either in ITRF94 or ITRF97 are necessary. The coordinates of the VLBI point can be used in equation (B-2), since the differences between the VLBI and the satellite reference points do not affect significantly. Since the transformation parameters of ITRF94 and ITRF97 are the same as seen in table B-3, the coordinates of Syowa VLBI reference point at 1998.9 is given by

X=1766194.152m, Y=1460410.940m, Z=-5932273.383m.

These values are used as $X_b(t)$ in equation (B-2). The transformation parameter sets are given by

$P_{94}(1990.1)=[0.67,\ 1.02,\ -0.88,\ 1.55,\ 0.00,\ 0.00,\ -0.14]$

$P_{97}(1990.1)=[0.67,\ 1.02,\ -0.88,\ 1.55,\ 0.00,\ 0.00,\ -0.14]$

$P_{94}(1999.9)=[0.67,\ 0.44,\ -2.26,\ 1.55,\ 0.00,\ 0.00,\ 0.06],$

$P_{97}(1999.9)=[0.67,\ 0.44,\ -2.26,\ 1.55,\ 0.00,\ 0.00,\ 0.06]$

Table B-4 shows the satellite determinations of the velocity of the Syowa space geodetic observation point expressed in ITRF2000.

Table B-4. The satellite determination of the velocity vector of the Syowa VLBI reference point in ITRF2000.

Source		V_X(cm/y)	V_Y(cm/y)	V_Z(cm/y)
IGS	NIPR/GSI	0.69	0.03	-0.41
DORIS	LEGOS/CLS	1.05	-0.62	0.25
	JPL	1.35	-0.53	-0.20

References

Argus, D. F. and Gordon, R. G. (1991): No-net-rotation model of current plate velocities incorporating plate model NUVEL-1, Geophys. Res. Let., 18, 2039-2042.

Argus, D. F. and Gordon, R. G. (1996): Test of the rigid-plate hypothesis and bounds on intraplate deformation using geodetic data from very long baseline interferometry. J. Geophys. Res., 101, 13555-13572.

Atlas Antarktiki (1966): Summarnaya solnechaya radiatsiya. Global Solar Radiation. year, 75-V, Moscow, Main Administration of Geodesy and Cartography of the Ministry of Geology, USSR, 225p.

Craddock, C. (1972): Geologic Map of Antarctica. New York, Am. Geogr. Soc.

Craddock, C. (1982): Antarctica and Gondwanaland. Antarctic Geoscience ed. by Craddock C., Madison, University of Wisconsine Press, 3-13.

Cretaux, J. -F., Soudarin, L., Cazenave, A. and Bouille, F. (1998): Present-day tectonic plate motions and crustal deformations from the DORIS space system. J. Geophys. Res.,

DeMets, C., Gordon, R. G. and Argus, D. (1988): Intraplate deformation and closure of the Australia-Antarctica-Africa plate circuit. J. Geophys. Res., 93, 11877-11897.

DeMets, C., Gordon, R. G., Argus, D. and Stein, S (1990): Current plate motions. Geophys. J. Int., 101, 425-428.

DeMets, C., Gordon, R. G., Argus, D. and Stein, S (1994): Effect of recent revisions to the geomagnetic reversal time scale on estimates of current plate motions. Geophys. Res. Let., 21, 2191-2194.

Diamond, P. J., Benson, J., Cotton, W. D., Wells, D. C., Romney, J. D. and Hunt, G. (1997): FITS Format for Interferometry Data Interchange. VLBA Correlator Memo, NRAO, June 10, 1997, 47p.

Fukuzaki, Y., Jike, T., Shibuya, K., Takashima, K., Maruyama, K., Iwata, A., Ishihara, M. and Doi, K (1999): On a geodetic soplution of the SYW991 Antarctic VLBI experiment. The 19th Symposium an Antarctic Geosciences Program and Abstructs, Oct, 14-15, 1999, NIPR, Tokyo, 1-2.

Grew, E. S. (1982): The Antarctic Margin. The Oceans Basins and Margins, 6, ed. by Narin, A. E. M. and Stehli, F. G., Plenum Pub., 697-755.

Gripp, A. E. and Gordon, R. G. (1990): Current plate velocities relative to the hotspots incorporating the NUVEL-1 global plate motion model. Geophys. Res. Let., 17, 1109-1112.

Heki, K (1999): Current motion of Antarctic Plate. Research meeting regarding to the Antarctic earthquake on Mar, 25, 1998 and evolution of Antarctic Plate, NIPR, Tokyo, Feb., 12, 1999.

Jike, T., Tanaka, T., Shibuya, K., Manabe, S., Tamura, Y., Sato, K., McCulloch, P., Costa, M., Nicolson, G., Quick, J. F. H., Shibata, K. M., Doi, K., Fukuzaki, Y., Jauncey, D. L. and Reynolds, J. (1999): VLBI Experiments at Syowa Station, Antarctica. Proceedings of the International Workshop on GEMSTON, Jan 25-28, 1999, CRL, Koganei, Tokyo.

Jike, T. (1999): The Activity Report of the Japan Antarctica Research Expedition 39th. The VLBI Observation and Hydrogen Maser, National Institute of Antarctic Research, 152-161.

Jike, T. (1999): Manual for Application of Syowa VLBI System. It is distributed to the VLBI observation member in charge of Syowa Station personally.

Kaminuma, K. (2000): A revaluation of the seismicity in the Antarctic. Polar Geosci., 13, 145-157.

Kaminuma, K., Kanao, M. and Kubo, A. (1998): Local earthquake activity around Syowa Station, Antarctica. Polar Geosci., 11, 23-31.

Kaminuma, K. et al. (1985): Science in Antarctica, 5, Tokyo, Kokin-shoin, 249-265.

Kanao, N., Shibuya, K., Watanabe, K., Fujiwara, S., Ikeda, H. and Okano, K (1995): A note on Geodetic Ties among Several Reference Points by Different Space Geodetic Techniques at Syowa Station, Antarctica. J. Geod. Soc. Japan, 41, 357-364.

Kawaguchi, N. and Kawano, N. (1978): bandwidth Synthesis techniques for precise delay measurement in VLBI. RRL Quarterly bulletin, 24, RRL.

Kojima, M. and Saito, T. (1978): Earth Period Learning. Iwanami-Kouza Chikyuu-Kagaku 6, Tokyo, Iwanami-Shoten Pub, 255p.

Kondo, T. (1982): Manual of software "KOMB", personal message.

Kubo, A., Nogi, Y. and Kaminuma, K. (1998): Systematic deviations of earthquake slip vectors from NUVEL1 at the Austraria-Antarctica and Pacific-Antarctica plate boundaries. Polar Geosci., 11, 61-75.

Kubo, A., Kanao, M., Hiramatsu, Y., Negichi, H. and Tono, Y. (1999): Shear wave splitting anisotropy beneath the Antarctic upper mantle and its possible formation processes. The 19th Symposium on Antarctic Geosciences Program and Abstracts, NIPR, Tokyo.

Kurihara, N., Ejiri, M., Takahashi, Takahashi, Y., Kondo, T., Koyama, Y., F., Jauncey, D. L. and Reynolds, J. E. (1995): The result of first Antarctic VLBI Experiments with Syowa Station in Antarctica, Antarctic Science.

Larson, K. M., Freymueller, J. and Philipsen, S. (1997): Global plate velocities from the Global Positioning System. J. Geophys. Res., 102, 9961-9981.

Larter, R. D. and Barker, P. F. (1991): Effects of the ridge crest-trench interaction on the young subducting plate. J. Geophys. Res., 96, 19583-19067.

McCarthy, D. D. (1996): IERS Technical Note 21. IERS Conventions, 95p.

Minstar, J. B. and Jordan, T. H. (1978): Present day plate motion. J. Geophys. Res., 83, 5331-5354.

Molnar, P., Atwater, T., Mammerickx, J. and Smith, S. M. (1975): Magnetic anomalies, bathemetry and the tectonic evolution of the Pacific since the late Cretaceous. Geophys. J. R. Astron. Soc., 40, 383-420.

Mori, K., Suga, H. and Uehara, M. (1992): Highly efficient Hydrogen Maser Atomic Frequency Standard. Anritsu Technical, Anritsu co. ltd., 63, 29-37.

National Institute of Antarctic Research (1991): Science in Antarctica 1 Introduction. Tokyo, Kokin-Shoin Pub, 295p.

National Institute of Antarctic Research (1985): Science in Antarctica 9 Data Compilation. Tokyo, Kokin-Shoin Pub, 288p.

Odamaki, M., Michida, Y., Noguchi, I., Iwanaga, Y., Ikeda and Iwamoto, K, (1991): Mean sea-level observed at Syowa Station, East Antarctica, Proceedings of the NIPR Symposium on Antarctic Geosciences, 5, 20-28.

Peltier W. R. (1994): Ice age paleotopoglaphy. Science, 265, 195-201.

Soudarin, L., Cretaux, J. –F. and Cazenave, A. (1999): Vertical crustal motions from the DIRIS space-geodesy system. Geophys. Res. Let., 26, 1207-1210.

Sovers, O. J. and Jacobs, C. S. (1996): Observation model and parameter partials for the JPL VLBI parameter estimation software "MODEST"-1996. JPL, NASA, Pasadena, JPL Pub., 83-39, Rev. 6, 151p.

Takahashi, Y. (1994): Estimation of errors in VLBI data and position. J. Geod. Soc. Japan, 40, 309-332.

Takahashi, F., Kondo, T. and Takahashi, Y. (1997): VLBI Technology. Tokyo, Ohmsha Pub., 258p.

Tamura, Y. (2000): Development of operating program for 11m antenna in Syowa Station, Antarctica, Geodetic VLBI experiment by very long baseline ties between the VLBI network in the south hemisphere and Japan, 25-57.

Tono, Y. and Kaminuma, K. (1998): A great earthquake in the Antarctic plate on 25 March 1998. Nankyoku Shiryo (Antarct. Rec.), 42, 190-195.

Tsuda, M., Suga, H., Urhara, M., Mori, K. and Kobayashi, M. (1990): Highly efficient Hydrogen Maser Atomic Frequency Standard. Anritsu Technical, Anritsu co. ltd., 60, 31-41.

Tushingham, A. M. and Peltier W. R. (1991): ICE-3G: A new global model of late Pleistocene Deglaciation based upon geophysical predictions of Post-Glacial relative sea level change. J. Geophys. Res., 96, 4497-4523.

Webb, P. N., Harwood, D. M., Mckelvey, B. C., Mabin, M. C. G. and Mercer, J. H. (1987): Late Cenozoic tectonic and glacial history of the Transantarctic Mountains. Ant. Jour. U. S., 21 (No. 5) (1986 Rev.), 99-100.

Wiens, D., Wysession, M. E., and Lawver, L. (1998): Recent oceanic intraplate earthquake in Balleny Sea was largest ever detected. EOS; Trans., 79, 353-354.

Yamada, A., Maruyama, K., Ootaki, O., Itabashi, A., Hatanaka, Y., Miyazaki, S., Negishi, H., Higashi, T., Nogi, Y., Kanao, M. and Doi, K. (1998): Analysis of GPS data at Syowa Station and IGS tracking stations. Polar Geosci., 11, 1-8.

Yoshida, Y. (1983): Physiography of the Prince Olav and the Prince Harald coasts, East Antarctica. Mem. Natl. Inst. Polar Res., Ser C, 13, 83.

Yoshida, Y. (1985): Science in Antarctica, 5, Tokyo, Kokin-shoin, 161-169